CHAPTER 2 ANALYSIS OF UWB MICROSTRIP ANTENNAS

2.1 Introduction

This chapter presents a brief description of UWB technology and elaborates its advantages, applications and challenges to design UWB antenna. It also provides details of different structures of planar monopole, fractal and dipole antenna. Various methods used to achieve UWB performance in those planar antenna structures are also discussed.

2.2 Advantages of UWB

UWB technology is providing a more significant solution to wireless communication systems in comparison to other technologies due to its several advantages as follows:

- **High data rate potential**

Since UWB covers a wide frequency spectrum, it can achieve huge channel capacity and high data rate in accordance with the Shannon-Hartley theorem. A capacity of hundreds of Mbps or several Gbps can be achieved for a distance between 1 to 10m.

- **Low interference**

The transmission power levels for UWB systems are extremely low. Due to the division of signal power across a wide frequency spectrum, the effect at any frequency is below the acceptable noise floor.

- **Security and reliability**

Due to low energy density, the UWB signal has "noise-like" shape. This noise-like shape makes the unintended detection very difficult. The interference caused because of real noise is required to spread uniformly over the entire frequency spectrum to affect the pulse. The noise can reduce the power level but cannot hinder the recovery of signal.

- **Multipath immunity**

Wide frequency spectrum of UWB signal reduces the time varying amplitude functions. Therefore, these signals have path delay approximately equal to 1 ns which is greater than pulse duration.

- **Immunity to fading**

The frequency diversity with minimal hardware offered by UWB systems increases the immunity to fading.

- **Potential small size and low equipment cost**

UWB system based on impulse radio features low cost and low complexity which arise from the essentially baseband nature of the signal transmission. UWB does not modulate and demodulate a complex carrier waveform, so it does not require components such as mixers, filters, amplifiers and local oscillators.

2.3 UWB Antenna Applications

As mentioned earlier in this chapter, UWB offers some unique and distinctive properties that make it attractive for various applications.

- ***Wireless Personal Area Network***

High data rate UWB has the potential for very high data rates using very low power at very limited range, which will lead to the applications well suited for WPAN.

- ***Sensor Networks***

A sensor network consists of a large number of nodes within a geographical area. The key requirements for sensor networks include low cost, low power and multi-functionality. These requirements can be fulfilled by using UWB technology. UWB systems are capable of gathering and disseminating or exchanging a vast quantity of sensory data in a timely manner. The cost of installation and maintenance will also drop significantly by using UWB sensor networks due to being devoid of wires. This merit is

especially attractive in medical applications because a UWB sensor network frees the patient from being shackled by wires and cables when extensive medical monitoring is required. In addition, with a wireless solution, the coverage can be expanded more easily and made more reliable.

- ***Positioning, Geolocation, Localization***

The high data rate characteristic of UWB technology in short range communication makes it capable of providing an excellent solution for indoor location with a much higher degree of accuracy of several centimeters. UWB systems can operate in complex situations to yield faster and more effective communication between people. They can also be used to find people or objects in a variety of situations, such as casualties in a collapsed building after an earthquake, children lost in the mall, injured tourists in a remote area, fire fighters in a burning building and so on.

- ***Imaging Applications***

UWB can also be applied to radar and imaging applications. It has been used in military applications to locate enemy objects behind walls and around corners in the battlefield. It has also found value in commercial use, such as rescue work where UWB radar could detect a person's breath beneath rubble, or medical diagnostics where X-ray systems may be less desirable.

2.4 UWB Antenna Challenges

UWB systems possess several advantages with great potentials as discussed in previously. The design of a suitable antenna is one of the several challenges required to be addressed for making UWB technology more effective. The challenges faced by antenna designers are as follows:

1. The antenna must operate over a frequency spectrum of 3.1-10.6 GHz with good impedance matching over a bandwidth of 7.5 GHz.

2. It should have also a stable radiation pattern across the whole UWB frequency range as well as an omni-directional radiation pattern to be suitable for short-range indoor wireless communication applications and mobile/portable devices.
3. The antenna should have constant group delay over the UWB frequency band. Constant group delay signifies linear antenna phase. The group delay and phase indicate how well an UWB pulse will be transmitted and to what degree it may be distorted or dispersed.
4. The requirements such as high efficiency, stable gain etc. as well as the physical constrains like physically small, planar to be applicable for recent mobile and portable devices are also very important.
5. The fidelity factor is a measure of distortion between two signals, preserving amplitude weighting and time shifting of the signal. It quantifies the distortion in the transmitted pulse caused by the antenna itself. The value of this factor should be close to 1 i.e. 100%.
6. The EIRP level of the designed antenna must comply with the FCC's emission levels, listed in Table 2.1 and Figure 2.1.

After the above discussion, it is thought useful to discuss about the various antenna geometries and methods used to design UWB antenna structures. In literature, several antenna structures like horn antenna, conical antenna, biconical antenna, spiral antenna, monopole antenna, dipole antenna, fractal antenna, Vivaldi antenna etc. are already discussed. Due to cost and size constraints, planar antenna structures like monopole antenna, fractal antenna, dipole antenna etc. are most commonly used. Therefore, a detailed study of different antenna geometries and methods is presented in the following sections.

Table 2.1 FCC emission limits for indoor and outdoor systems

Frequency range (MHz)	Indoor emission mask (dBm/MHz)	Outdoor emission mask (dBm/MHz)
960-1610	-75.3	-75.3
1610-1900	-53.3	-63.3
1900-3100	-51.3	-61.3
3100-10600	-41.3	-41.3
above 10600	-51.3	-61.3

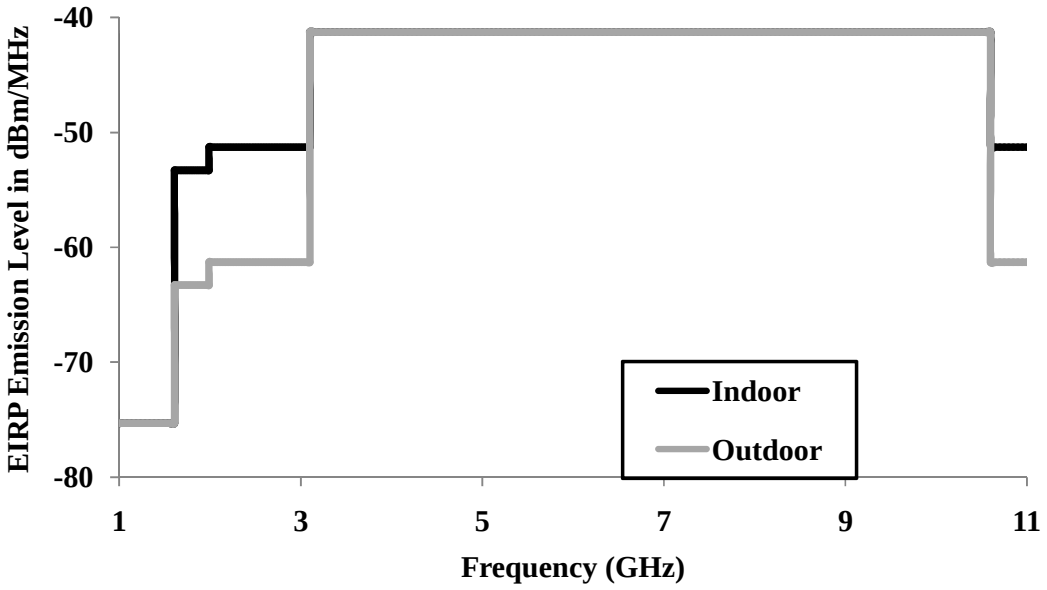

Figure 2.1 FCC's indoor and outdoor emission masks

2.5 Monopole Antenna

Basically, a monopole antenna is a λ/4 long electrical conductor mounted above the ground plane. It is also called as quarter wave monopole. Its length is half of dipole antenna. The basic dipole antenna is shown in Figure 2.2(a). Using image theory, the fields above the ground plane can be found by using the equivalent source (antenna) in free space as shown in Figure 2.2(b). This is simply a dipole antenna of twice the length. The fields above the ground plane in Figure 2.2(a) are identical to the fields in Figure 2.2(b), which are known. The monopole antenna fields below the ground plane in Figure 2.2(a) are zero.

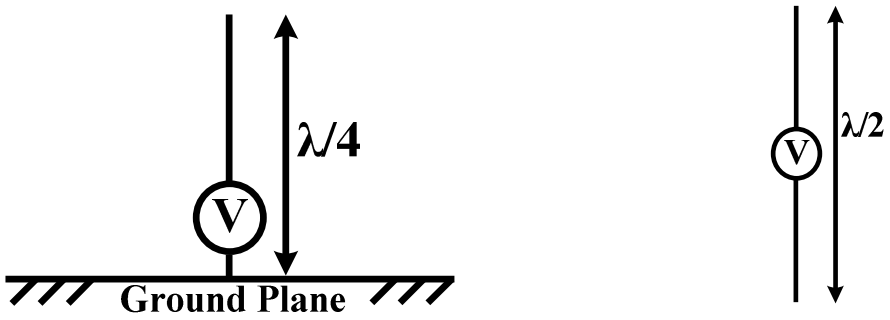

(a) (b)

Figure 2.2 (a) Monopole above a conducting ground plane, (b) the equivalent source in free space

Planar monopole antennas have several advantageous features like wide impedance bandwidth, nearly omnidirectional azimuthal radiation pattern, easy to fabricate, cost effective, easy integratability etc.

Monopole antennas, having omni-directional radiation pattern characteristics, are very suitable for indoor applications, such as airplane, shopping center, hospital, etc. Particularly, their directivity on or near the radio horizon makes them suitable for communication systems where maximum operational range often depends on the directivity on the radio horizon.

While designing UWB monopole antenna, instead of resonance or operating frequency, lower band-edge frequency and total bandwidth achieved become the design parameters. The lower band edge frequency depends primarily on maximum height of the monopole, whereas bandwidth of the antenna depends on how impedance of various modes is matched with the microstrip or coplanar feed line. The details of design techniques used for impedance bandwidth enhancement, radiation pattern improvement, mathematical analysis etc. while fabricating UWB monopole antenna already reported in the literature are presented as follows:

2.5.1 Monopole antenna with modified feedline structures

1. Double feed structure [27, 119], shown in Figure 2.3, is used for generation of pure and intense vertical current distribution to decrease the cross-polar component and to prevent the excitation of other modes. According to the Theory of Characteristic Modes, the insertion of two symmetric feed ports prevents the excitation of horizontal currents and assures that only the dominant vertical current mode is present in the structure resulting into an improvement in the polarization properties and impedance bandwidth.
2. Defective microstrip structure(DMS) [81, 224], shown in Figure 2.4, is achieved by introducing defect in the feed line. It increased the electrical length of the antenna to make it a part of the radiator and not only a feeding line. The DMS element acted as a radiating slot which resonates at lower frequencies suggesting that the wideband characteristics are due to the overlapping of the resonance of DMS and planarized monopole. Due to the slot in the feed-line, the inductive and capacitive properties of the input impedance got changed resulting into enhanced antenna bandwidth.
3. Trident-shaped strip and a tapered impedance transformer [103] are used to achieve the uniform omnidirectional H-plane patterns at higher frequencies by neglecting the cross polar components generated due to partial ground plane having width comparable to the wavelength at those frequencies. Due to this ignorance of cross-polarization components, its vertical surface current distributions will mainly determine its horizontal radiation patterns. This may lead to stronger radiation in the broadside due to contributions of all the vertical surface currents which are in-phase or nearly in-phase within the impedance bandwidth and weaker radiations in some directions due to the planar structure

resulting into out-of-phase vertical surface currents for a planar monopole antenna. The monopole antenna with trident-shaped strip and a tapered impedance transformer is shown in Figure 2.5(a).

(a) (b)

Figure 2.3 Monopole antenna structures with double feed

(a) (b)

Figure 2.4 Monopole antenna structures with Defective microstrip structure(DMS)

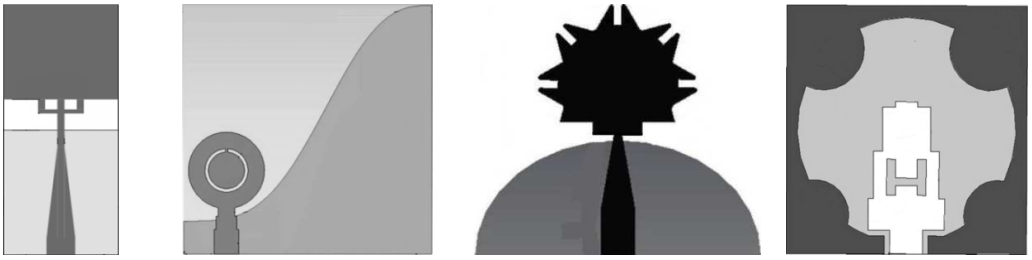

(a) (b) (c) (d)

Figure 2.5 Monopole antenna with (a) Trident-shaped strip and a tapered impedance transformer, (b) Stepped impedance transformer, (c) Tapered feedline, and (d) Staircase subtractive stripline loaded with slot

4. Stepped impedance transformer [272] is designed by dividing the feedline in to three-sections having different widths. The width of each section is optimized parametrically for better impedance matching over wide spectrum of UWB specifications. The antenna structure having stepped impedance transformer is illustrated in Figure 2.5(b)
5. Tapered feedline [277], demonstrated in Figure 2.5(c), is utilized to achieve smooth transition among the higher modes from feedline to radiating patch.
6. Staircase subtractive stripline loaded with slot [286], presented in Figure 2.5(d), improved the impedance matching by the creation of an additional surface current path along the slot and causing more current surface.

2.5.2 Monopole antenna with electromagnetic band gap (EBG)

To enhance the impedance bandwidth [167] or to reject interfering frequency bands [164, 185], electromagnetic band gap structures are embedded around the feedline, on the patch or in the ground plane. The proposed technique had many advantages, such as notch-frequency tunability, notch-band width controllable capacity, efficient dual-notch design and stable radiation patterns. Some monopole antenna structures are shown in Figure 2.6, 2.7 and 2.8. Mushroom like EBG structure was composed of metallic patches connected to the ground plane by using vias. Its operation was represented by an LC filter array (shown in Figure 2.6). The inductor L, due to currents flowing through vias and the capacitor C, due to the gap between two patches were approximated by the following equations:

$$\omega_o = \frac{1}{\sqrt{LC}} \tag{1}$$

$$L = \mu_o h \tag{2}$$

$$C = \frac{W\varepsilon_o(1+\varepsilon_r)}{\pi} cosh^{-1}\left(\frac{W+g}{g}\right) \quad (3)$$

$$BW = \frac{\Delta\,\omega}{\omega_o} = \frac{1}{\eta}\sqrt{\frac{L}{C}} \quad (4)$$

Where,

h	=	substrate thickness
ε_r	=	dielectric constant of the substrate
W	=	width of EBG
g	=	gap of EBG
ω_o	=	centre frequency of the notched band
BW	=	bandwidth of the notched band
η	=	free-space impedance

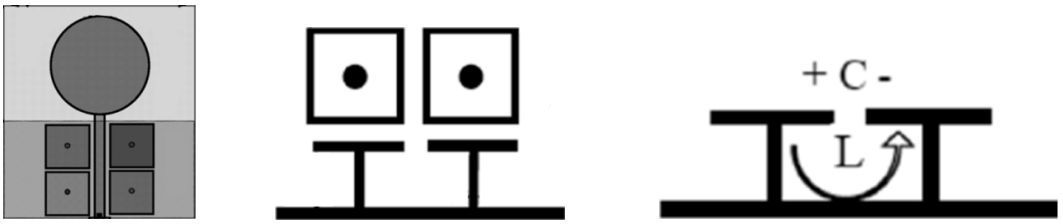

(a) (b) (c)

Figure 2.6 (a) Geometry of the proposed UWB antenna with EBG. (b) Unit cells of EBG. (c) Equivalent circuit of the EBG.

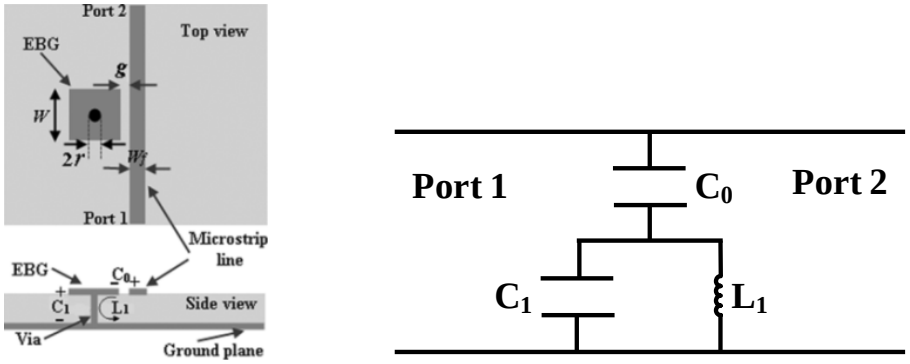

(a) (b)

Figure 2.7 (a) Bandgap for the mushroom-type EBG in terms of W. (b) Effect of the coupling gap on the width of the bandgap.

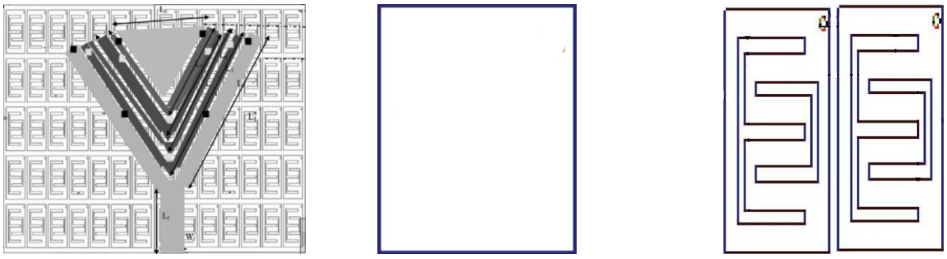

(a) (b) (c)

Figure 2.8 The unit cell shapes (a) Antenna with EBG array (b) conventional shape and (c) new EBG shape

2.5.3 Monopole antenna designed using Genetic Algorithm (GA)

Genetic Algorithm (GA) uses a matrix-based chromosome to describe the shape of the planar monopole element to achieve the desired performance [52, 80]. The GA optimizer minimizes the some cost function to optimize the impedance matching and radiation pattern simultaneously. The monopole antenna designed using GA are illustrated in Figure 2.9.

$$C = w_1.C_1 + w_2.C_2 + w_3.C_3 \tag{5}$$

$$C_1 = \begin{cases} max_{f\in F_m}\{\rho(f) - \rho_{m,goal}\}, & if \exists \rho(f) > \rho_{m,goal} \\ 0, & otherwise \end{cases} \tag{6}$$

$$C_2 = \begin{cases} max_{f\in F_u}\{\rho_{u,goal} - \rho(f)\}, & if \exists \rho(f) < \rho_{u,goal} \\ 0, & otherwise \end{cases} \tag{7}$$

$$C_3 = \begin{cases} max_{f\in F}\{G_{dev}(f,\theta) - G_{dev,goal}\}, if \exists G_{dev}(f,\theta) > G_{dev,goal} \\ 0, \quad otherwise \end{cases} \tag{8}$$

Where,

$C_1, C_2\ and\ C_3$	=	Cost function
$w_1, w_2\ and\ w_3$	=	relative weight of each cost function term
F_m	=	set of well matched frequencies in the operating band
F_u	=	set of frequencies in the notch band
$G_{dev}(f,\theta)$	=	maximum deviation in gain between any two azimuth angles for a given frequency f, and elevation angle θ
$\rho_{m,goal}, \rho_{u,goal}, G_{dev,goal}$	=	constraints prevent the GA from optimizing $C_1, C_2\ or\ C_3$ more than is needed

Since the optimization process of genetic algorithm (GA) requires impractical run-time for designing the UWB antennas with the band-notched function because the GA with small population size exhibits poor convergence and the evaluation of one fitness function requires a long time. The micro-genetic algorithm (MGA) was found to be computationally more efficient for small populations. The MGA and FDTD methods were combined [105] to design a band-notch UWB monopole antenna composed of a stepped U-type monopole loaded with an U-type slot for WLAN band notch-characteristic. The combination of MGA and FDTD improved the global and local searching ability efficiently, avoided the premature convergence and obtained the global optimal solution with a small population. The fitness function used was as follows:

$$fitness = w_1 * c_1 + w_2 * c_2 \tag{9}$$

$$c_1 = \frac{1}{M}\sum_{f=3.1GHz}^{5.15\,GHz} VSWR1(f) + \frac{1}{N}\sum_{f=5.825GHz}^{10.6\,GHz} VSWR1(f) \tag{10}$$

$$c_2 = P - \sum_{f=5.15GHz}^{5.825\,GHz} VSWR2(f) \tag{11}$$

$$VSWR1(f) = \begin{cases} VSWR, & VSWR \geq 2 \\ 2, & VSWR < 2 \end{cases} \tag{12}$$

$$VSWR2(f) = \begin{cases} VSWR, & VSWR \leq 3.5 \\ 3.5, & VSWR > 3.5 \end{cases} \tag{13}$$

Where,

w_1 and w_2 = weights of c_1 and c_2,
M and N = No. of samples in the bands of 3.1-5.15GHz and 5.825-10.6 GHz
P = constant relative to the samples within 5.15-5.825GHz.

The combination of the Jumping Genes (JG) genetic operator and the non-dominated sorting genetic algorithm II (NSGA-II) was utilized [106] to design an UWB planar multiple-trapezoidal monopole antenna with the rectangular/rounded-corner

ground plane to meet multiple UWB antenna design performance requirements like minimum VSWR, minimum antenna size, minimum variation of radiation pattern, uniform radiation pattern and uniform gain, over the whole frequency band simultaneously.

The NSGA-II multi-objective optimization evolutionary algorithm (MOEA) adopts the fast non-dominated sorting approach, crowding mechanism, and elitism strategy by combining the parent and offspring populations and selecting the best N solutions (where N is the population size).

The JG's perform a horizontal genes transmission that allows the genes to jump over from one position to another position within the same chromosome or even to another chromosome in the population pool, whereas the usual genetic operations such as crossover and mutation provide only the chromosome improvement in vertical transmission. The transposition operation procedures are implemented between the selection and the crossover processes. The cut-and-paste and copy-and-paste transposition are chosen randomly similar to crossover and mutation. In cut-and-paste operation, the transposon (jumping gene) gets cut from one location and pasted to another in a chromosome; whereas in copy-and-paste transposition the transposon replicates itself, and the copy is inserted into a new location. The jumping genes genetic algorithm (JGGA) is robust and provides outcomes in speed with accuracy. It has two distinct advantages: (i) it can extend the diversity of non-dominated solutions along the Pareto-optimal front; and (ii) the non-dominated solutions can converge quickly into the Pareto-optimal front.

The performance of the planar monopole antenna was improved by developing a JGGA optimizer by coding all the real numbers, obtained by coding all tunable parameters of the antenna, in one chromosome and ranging each gene between 0 and 1.

The practical value x_i of the ith parameter of the antenna was obtained from the following:

$$x_i = \left(x_{i,max} - x_{i,min}\right) \times a_i + x_{i,min} \tag{14}$$

Where,

a_i = value of the i^{th} gene of a chromosome
x_i = parameter whose range lies between $x_{i,max}$ and $x_{i,min}$

For achieving above mentioned desired performances, five objective functions as follows were defined:

$$minimize\ F_1 = \underset{f \in F_m}{max}\{VSWR(f)\} \tag{15}$$

$$minimize\ F_2 = width \times length \tag{16}$$

$$minimize\ F_3 = \frac{1}{2M(N-1)} \sum_{\varphi=\left\{0,\frac{\pi}{2}\right\}} \sum_{j=1}^{M} \sum_{k=1}^{N-1} \left|E\left(f_j, \theta_{k+1}, \varphi\right) - E\left(f_j, \theta_k, \varphi\right)\right| \tag{17}$$

$$minimize\ F_4 = \frac{1}{2(M-1)N} \sum_{j=1}^{M-1} \left| \sum_{\varphi=\left\{0,\frac{\pi}{2}\right\}} \sum_{k=1}^{N} E\left(f_{j+1}, \theta_k, \varphi\right) - \sum_{\varphi=\left\{0,\frac{\pi}{2}\right\}} \sum_{k=1}^{N} E\left(f_j, \theta_k, \varphi\right) \right| \tag{18}$$

$$minimize\ F_5 = \underset{f \in F_m}{max}\{Gain(f)\} - \underset{f \in F_m}{min}\{Gain(f)\} \tag{19}$$

Where,

$VSWR(f)$ = VSWR at frequency f
F_m = set of sampled frequencies
$\left|E\left(f_j, \theta_{k+1}, \varphi\right) - E\left(f_j, \theta_k, \varphi\right)\right|$ = absolute difference of the radiated electric fields
$Gain(f)$ = maximum directive gain of the antenna

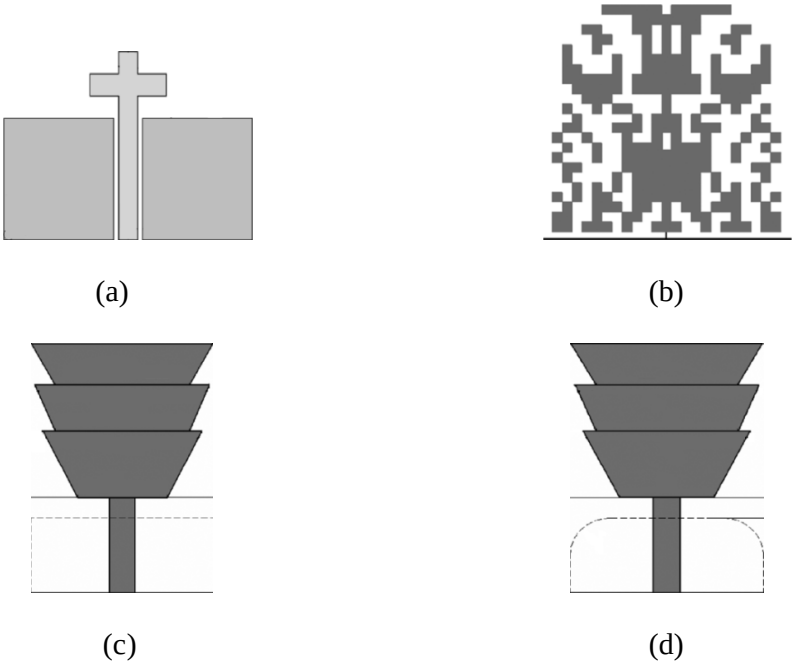

(a) (b)

(c) (d)

Figure 2.9 Monopole antenna designed using Genetic Algorithm (GA)

2.5.4 Monopole antenna analyzed using FDTD

The Finite Difference Time Domain (FDTD) method, a time domain technique, directly calculates the impulse response of an electromagnetic system implying that a single simulation can provide Ultrawideband temporal waveforms. It is found to be more suitable than the frequency domain method in designing the wide-band antenna [52]. The numerical analysis of an UWB microstrip-fed tap monopole antenna [66], shown in Figure 2.10(b), was carried out by using finite-difference time domain (FDTD) method [67]. The antenna structures are demonstrated in Figure 2.10.

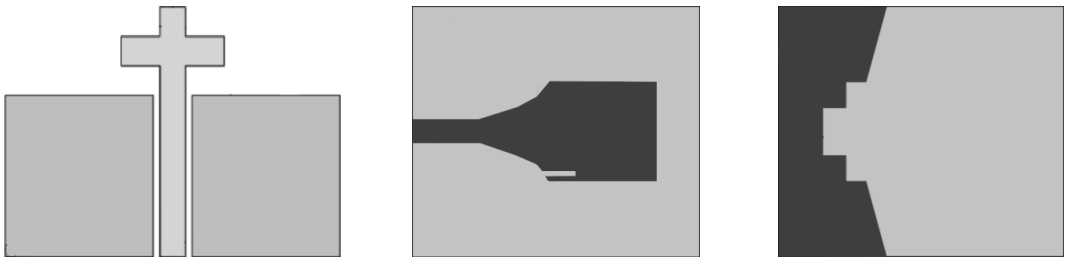

(a) (b) (c)

Figure 2.10 Monopole antenna analyzed using FDTD

2.5.5 Monopole antenna with conductor backed plane

Another method of impedance bandwidth enhancement or band rejection function is the use of conductor backed plane. It improved the electromagnetic coupling between the patch and ground plane which results into bandwidth enhancement [144]. In another case, it perturbed the resonant response and also acted as a parasitic half-wave resonant structure electrically coupled to the rectangular monopole. Since the current flow around the parasitic element were more dominant and opposite to that of radiating patch at the notch frequency, the desired high attenuation near the notch frequency was produced [101, 124, 224]. Few antenna configurations are illustrated in Figure 2.11.

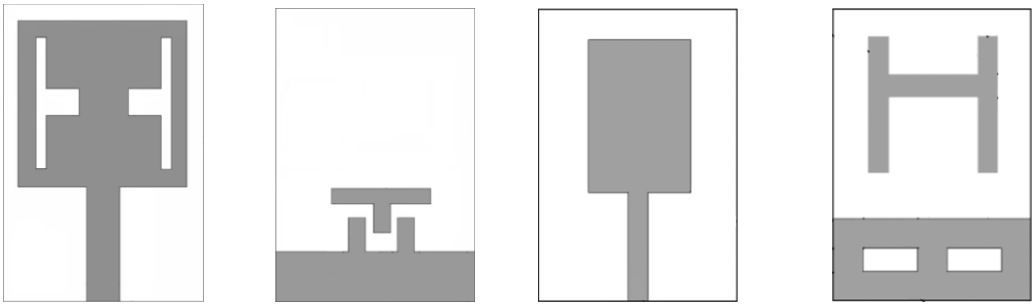

(a) (b) (c) (d)

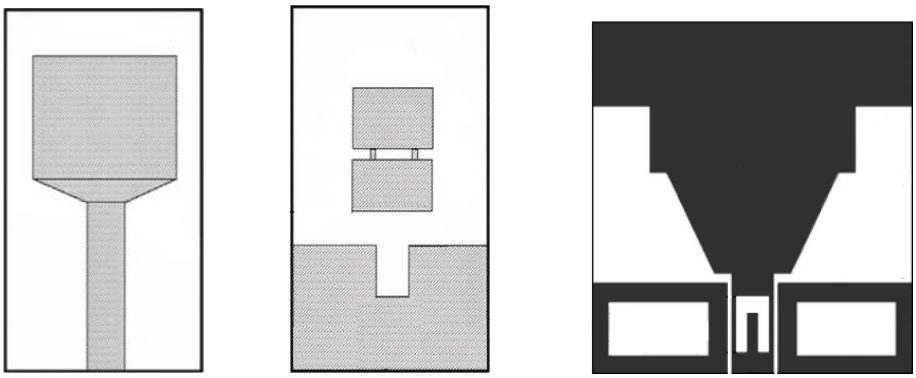

(e) (f) (g)

Figure 2.11 Monopole antenna with conductor backed plane

2.5.6 Monopole antenna with defected ground structures

According to Babinet's Equivalence Principle, the truncated ground plane helps matching the patch with the feedline in a wide range of frequencies. This is because the truncation creates a capacitive load that neutralizes the inductive nature of the patch to produce nearly pure resistive input impedance. The lower frequency bandwidth is significantly affected by using the notch in the ground plane and the upper frequency bandwidth is sensitive to the notch on the radiating patch. This behavior is mainly due to the change of surface current path by the dimensions and locations of notches. The ground plane slots provide an additional current path and result in change of inductance and capacitance of the input impedance leading to change in impedance bandwidth [101, 158, 224].

The bandwidth of a conventional planar triangular monopole antenna was enhanced [91] by introducing the ridged ground planes with two symmetrically hillside-shaped corrugations. The triangle ridged and trapezoid-ridged shapes provided a smooth transition from the feeding line to the radiating element which resulted into enhancement of impedance bandwidth. The triangle shaped corrugations of the ridged ground had a function similar to the sleeve in the sleeve monopole antenna. Two additional resonant modes above the fundamental one were excited at nearby frequencies with good impedance matching. Two symmetrical antipodal tapered slot-structures antennas (ALTSA) had been observed comprising the triangular plate and the ridged ground plane. So the planar triangular monopole antenna (PTMA) with ridged ground had three resonant modes. The ridged ground plane did not affect the lower-edge frequency of PTMA significantly. The printed PTMA with the ridged ground plane had slightly higher antenna gains. Antenna structures are depicted in Figure 2.12.

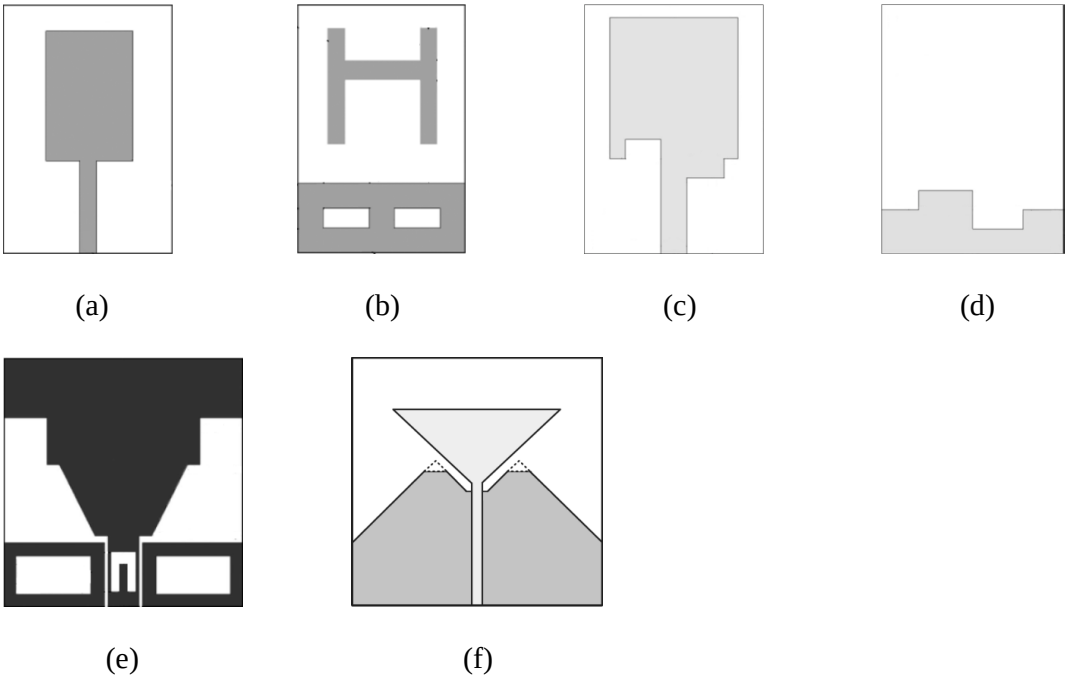

Figure 2.12 Monopole antenna with defected ground structures

2.5.7 Monopole antenna with slot loaded patch

A circular-ring UWB monopole antenna [43] was derived by removing the central part of circular disc monopole antenna [35]. The central portion of the disc was removed due to the fact that the current distributes mainly along the edge and the central part has very low current density.

Two CPW-fed UWB elliptical monopoles with reconfigurable band rejection characteristic in the frequency band of 5-6 GHz (HIPERLAN/2 and WLAN) were designed [122]. The band rejection characteristic had been achieved by using a $\lambda/2$ long U-shaped slot in one antenna and a pair of $\lambda/4$ long inverted L-shaped stubs placed symmetrically in second antenna, acting as resonating elements. The reconfigurability had been introduced by using the micro-electro-mechanical system (MEMS) switches to activate and deactivate the resonating elements without the need of dc bias lines. The lack of bias lines for the MEMS switches made the fabrication easier and improved the radiation performance of the antenna, since there is no coupling or

leakage from the bias lines. For the first antenna, a U-shaped slot was loaded on the monopole and a MEMS switch was used to short the resonant slot when the band rejection is not required. For the second antenna, two inverted L-shaped open circuit stubs were symmetrically placed near the elliptical radiator. MEMS switches were used to connect stubs to the radiator when the band rejection was required. The U-shaped slot resonated and therefore created a band notch at the frequency defined by

$$f_U \sim (c/4(L_{S1} + (W_{S1}/2) - G_{S1})) \tag{20}$$

Where,

c = speed of light
L_{S1} = length of each vertical arm
W_{S1} = width of the U slot
G_{S1} = width of each vertical arm

The U-shaped slot was modeled as a $\lambda/4$ long, short circuit terminated series stub similar to a spurline filter by using the transmission line model. The MEMS switch was across the input to the series stub. When the switch was open, as shown in Figure 2.13, the spurline filter was in the circuit, and the signal got reflected at the stub resonant frequency due to an equivalent series open circuit. While for the case of closed switch, the spurline filter got shorted and removed from the circuit resulting in radiation at all frequencies. Similarly, the inverted L-shaped open-circuit terminated stubs resonated at

$$f_{inverted\_L} \sim \frac{c}{4(L_{S2} + W_{S2})} \tag{21}$$

Where,

L_{S2} = length of vertical arm
W_{S2} = length of horizontal arm

The bandwidth of a microstrip line fed square monopole antenna is enhanced by loading the patch with T-shaped slots and introducing a pair of rectangular sleeve on the

ground plane with a T-shaped conductor-backed plane [144]. The T-slots were introduced on the observation that the current distribution at low frequency was along the vertical plane at the monopole's bottom edge and along the horizontal plane at higher frequency in UWB frequency band. The antenna structures are presented in Figure 2.14.

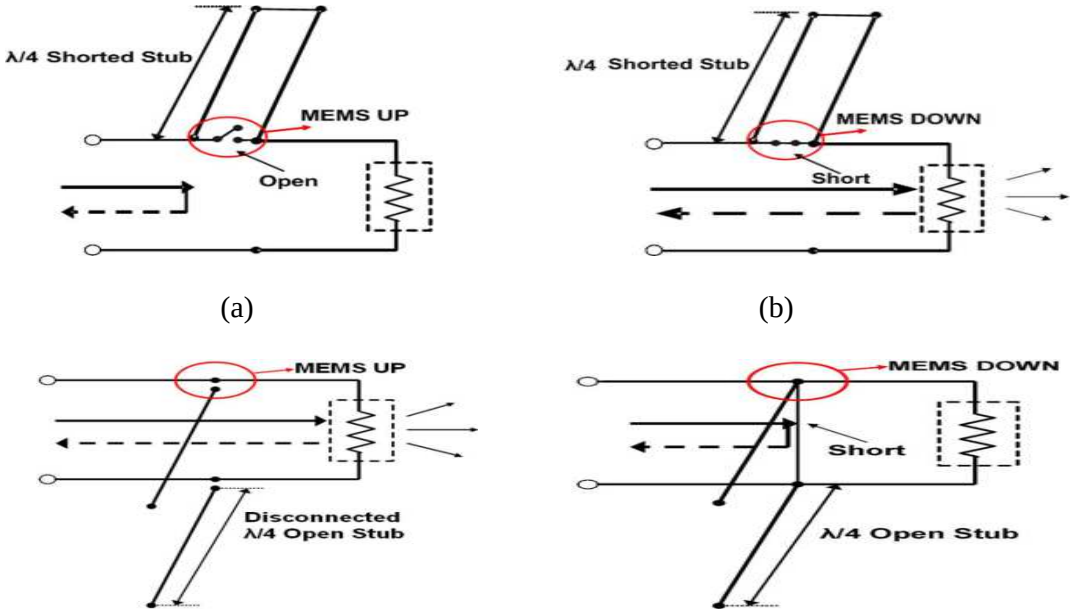

Figure 2.13 Transmission line model for (a) U-shaped slot with MEMS up, (b) U shaped slot with MEMS down, (c) inverted L stubs with MEMS up, (d) inverted L stubs with MEMS down.

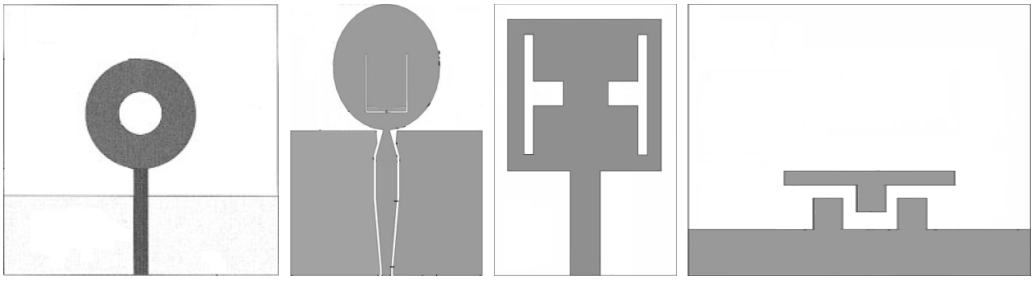

Figure 2.14 Monopole antenna with slot loaded patch

2.5.8 Monopole antenna with parasitic patch

The addition of a parasitic patch improved the impedance bandwidth of monopole antenna structures [140, 156, 274]. The impedance bandwidth got enhanced due to the fact that the electric field density increases on placing a parasitic patch between the main radiator and the parasitic patch due to capacitive loading. This capacitive loading resulted into increase in the electrical length of the antenna leading to the lowering of the lower-band edge frequency. In case of stacked parasitic patch, the source-driven patch interacted with the parasitic patch placed strategically on top of the fed patch. When the distance between the patches was less, these patches formed a leaky resonator whose resonant fields enhanced the antenna's gain. Some antenna structures are shown in Figure 2.15.

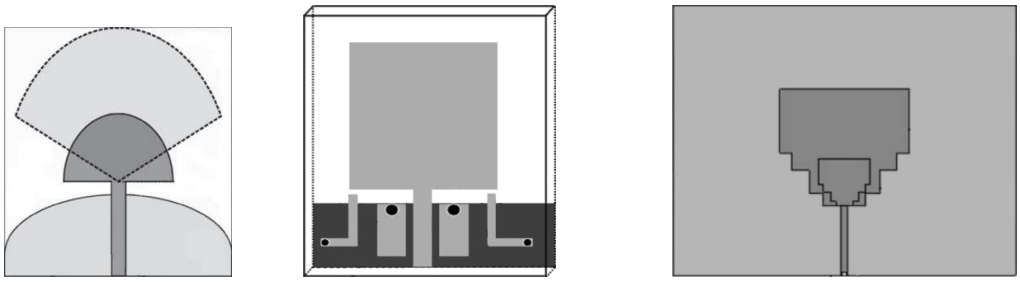

(a) (b) (c)

Figure 2.15 Monopole antenna with parasitic patch

2.5.9 Effect of feed gap on monopole performance

The impedance bandwidth of monopole antenna is found to be very much dependent on the gap between the feedline and ground plane [31, 286]. This gap is responsible for the electromagnetic coupling between them which results in the tuning of impedance matching. Some antenna configurations are illustrated in Figure 2.16.

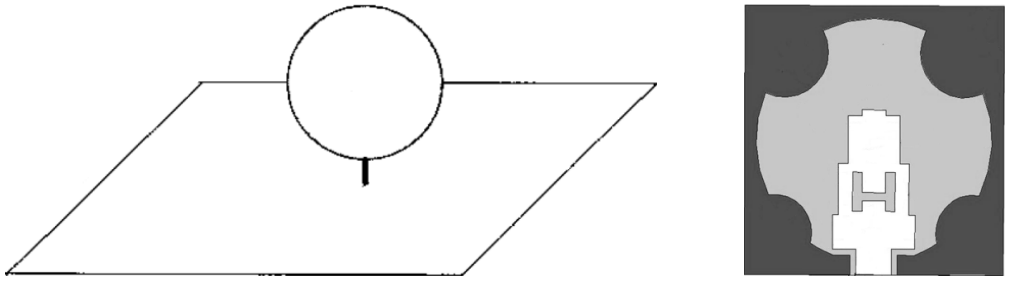

(a) (b)

Figure 2.16 Effect of feed gap on monopole performance

2.5.10 Monopole antenna with equivalent circuit

The pair of coupled lines in fork shaped radiator, used to achieve band notch characteristics, was modeled by using one-port network composed of a coupled-line section and a finite-size ground plane with a delta source excitation. An equivalent circuit model had been investigated by representing each coupled line by a lumped parallel lossy RLC circuit, strip by an inductive load and tapped line by inductive and capacitive loads considering their distributive nature [88, 137, 146]. The antenna input admittances had been calculated in terms of J-inverter and conductance. To achieve equivalent circuit model of a multiple band notch antenna, the radiating element was modeled as a series of parallel RLC resonance elements, the notched bands were modeled as short circuited series and shunt type stubs and the CPW-feed line as a transmission line with characteristic impedance Z_o [205]. The higher order modes of elliptical antenna structure had been represented in complete Foster canonical form by a series of parallel RLC components [170]. The antenna configurations and their equivalent circuits are depicted in Figure 2.17-2.22.

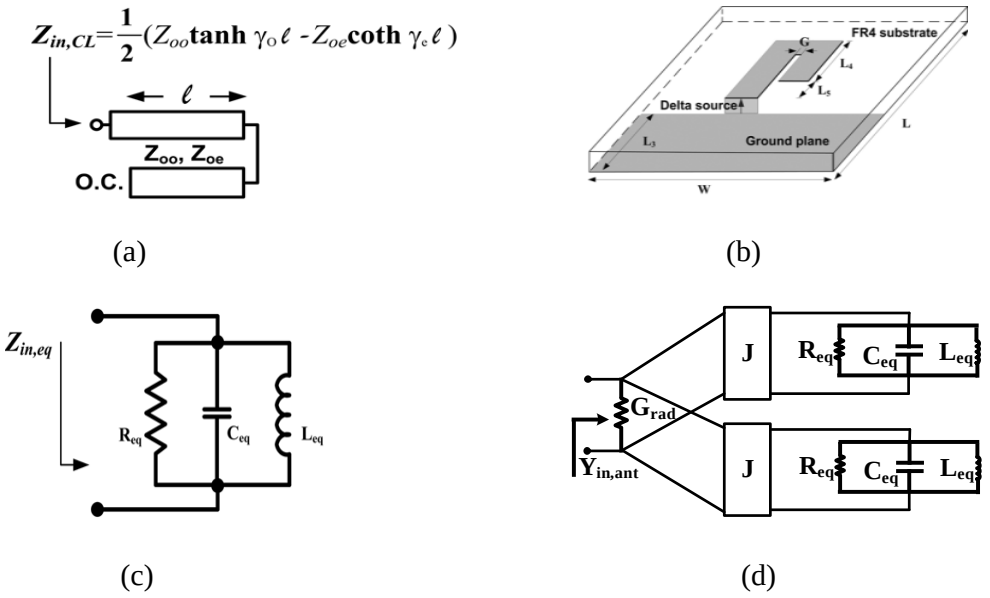

Figure 2.17 (a) Schematic diagram of the coupled lines. (b) Circuit layout for extracting the lumped equivalent circuit model in (c). (c) Lumped equivalent circuit model of the coupled-line section. (d) Equivalent circuit model of the proposed antenna.

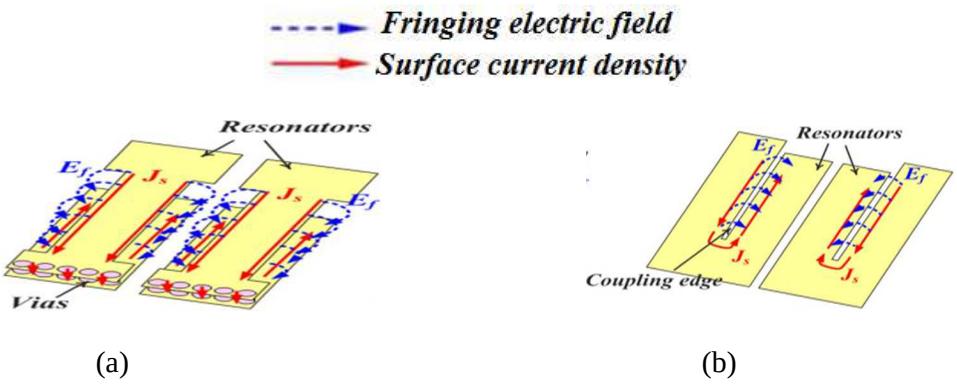

Figure 2.18 Electric fields and surface current distributions on the (a) vertically and (b) horizontally arranged folded-strip resonators.

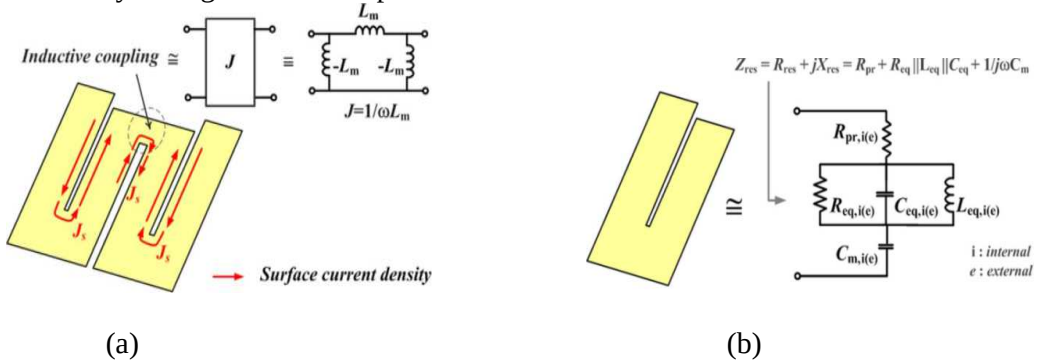

Figure 2.19 (a) Inductive coupling scheme and its equivalent circuit model, (b) Novel equivalent circuit model for the folded-strip resonator

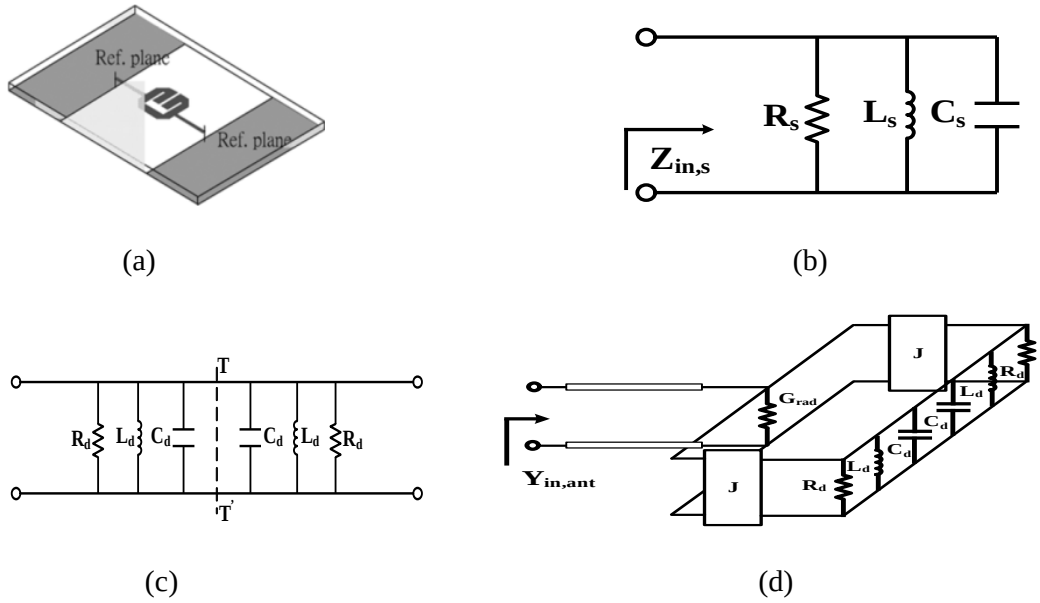

Figure 2.20 (a) Exacting structure of the proposed resonator. (b) One-port lump equivalent circuit network of the proposed resonator. (c) Two-port lump equivalent circuit network of the proposed resonator. (d) Simplified equivalent circuit model of the proposed antenna.

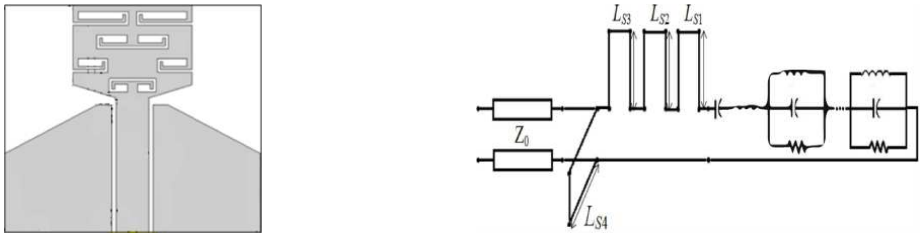

Figure 2.21 Geometry of the proposed multi band-notch antenna (a) Patch antenna loaded with slots, (b) The equivalent circuit model for the proposed multi-band notch antenna

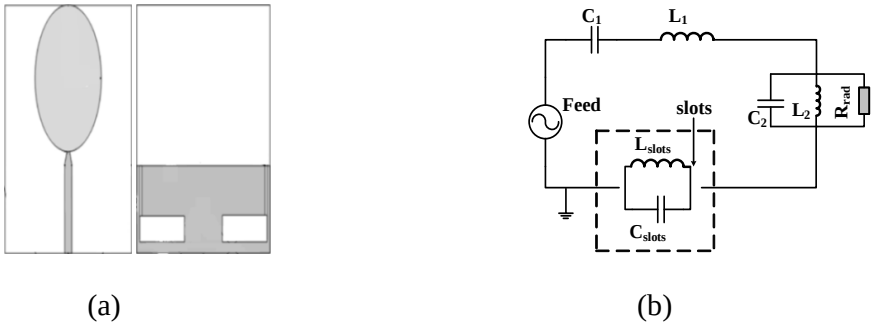

Figure 2.22 (a) Geometry of the proposed UWB elliptical monopole antenna: front view, back view, and side view. (b) Equivalent circuit of the proposed UWB antenna

2.5.11 Monopole antenna with split resonators

The split ring resonator (SRR) placed close to the feed line gets strongly coupled to it. It creates band notched frequency filter by capturing and storing all of the input energy at its resonance frequency. SRR structures are modeled by using combination of equivalent inductive and capacitive loads coupled to each other [258, 270]. Some antenna structures are presented in Figure 2.23.

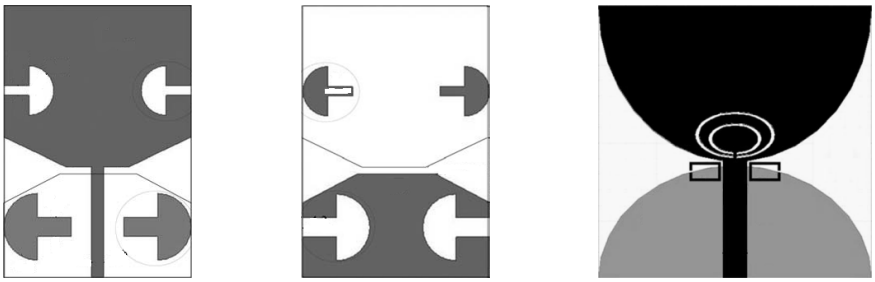

(a) (b) (c)

Figure 2.23 Monopole antenna with split resonators

2.6 Fractal Antenna

According to Webster's Dictionary a fractal is defined as being "Derived from the Latin *'fractus'* meaning broken, uneven. The term fractal was originally coined by Mandelbrot to describe a family of complex shapes that possess self-similarity or self-affinity in their geometrical structure. Self-similarity means each part of the shape is a smaller version of the whole shape. Another property of fractal is space filling that means the size of fractal structure becomes large in the same area as the number of iterations increase. Because of this property fractal geometries have been applied to antenna design to make multiband and broadband operational antenna. [303-304]

2.6.1 Fractal in Nature

Any of various extremely irregular curves or shapes that repeat themselves at any scale on which they are examined can be considered as a fractal. Fractals permeate

our lives, appearing in places as tiny as the membrane of a cell and as majestic as the solar system. Fractals are the unique, irregular patterns left behind by the unpredictable movements of the chaotic world at work. In universe, everything existent is a fractal for example:

- The leaves in trees,
- The veins in a hand,
- Waters swirling and twisting out of a tap,
- A puffy cumulus cloud,
- Tiny oxygen molecule, or the DNA molecule [461].

2.6.2 Properties of Fractal Antenna

Any Fractals are used as antenna elements due to their following properties:

- ***Fractals as Space-filling Geometries***

Space-filling properties lead to curves that are electrically very long, but fit into a compact physical space and can lead to the miniaturization of antenna elements.

- ***Fractals as Miniaturized***

A fractal can fill the space occupied by the antenna in a more effective manner than the traditional Euclidean antenna. This leads to more effective coupling of energy from feeding transmission lines to free space in less volume.

- ***Fractals as Multiband***

Fractal antenna represents a class of electromagnetic radiators where the overall structure is comprised of a series of repetition of a single geometry and where repetition is at different scale. In order to enable more operating bands within lower spectrum, a higher scaling factor is required. [461]

2.6.3 Fractal Antenna Geometries

Iterative function system (IFS) is the general method to describe the fractal structure, it creates a series of self-affine on the basis of transformation W, the W can be formulated as:

$$W\begin{pmatrix} x \\ y \end{pmatrix} = \begin{pmatrix} a & b \\ c & d \end{pmatrix}\begin{pmatrix} x \\ y \end{pmatrix} + \begin{pmatrix} e \\ f \end{pmatrix} \tag{22}$$

Where the *a, b, c, d, e* and *f* are real numbers. The *a, b, c* and *d* control the rotation and scale transformation; the *e* and *f* control linear shift. Assume w_1, $w_2 \ldots w_n$ are a series of linear affine transformation and the A represents the initial graph. By application transform of A, it can be expressed as follow:

$$W(A) = \bigcup_{n=1}^{N} w_n(A) \tag{23}$$

The fractal geometry is generated by using Hutchinson operator, W. IFS fractal is a powerful tool in antenna design. It provides a description, classification and operation of the general method of fractal. There are many fractal geometries those have been discovered and investigated to be useful in developing new and innovative designs for antennas. Some of unique geometries are being discussed below. [462]

2.6.3.1 Appollian gasket fractal

It is one of the best known circle inversion fractals. Circle inversions are carried out iteratively on three mutually tangent circles having same radius to design these fractals. It is designed by three mutually tangent circles, and drawing the inner Soddy circle. Thereafter, the inner Soddy circle of this circle is drawn with each pair of the original three circles and this is continued iteratively. Three initial circles are surrounded by another Soddy circle and the additional gaps are filled with inner Soddy

circles to form the Apollonian gasket. The stepwise design of Appollian gasket is illustrated in Figure 2.24 [386, 463].

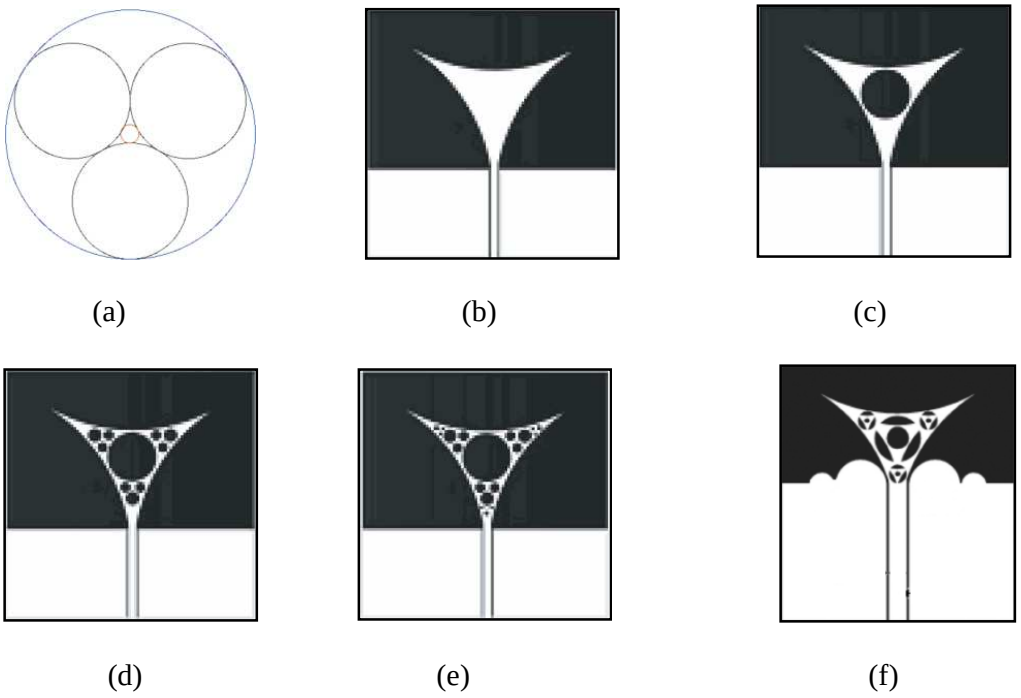

Figure 2.24 Appollian gasket geometries.

2.6.3.2 Minkowski Fractal Geometry

Similar to all fractals curves, the designing of Minkowski curve is also based on a recursive procedure. At each recursion, an 8-sided or 5-sided generator is applied to each line segment of the curve. It starts from a straight line. The same generator is applied to the 8/5 segments formed at the first iteration to produce a somewhat more complex curve [401-403, 410]. Some of the Minkowski fractal antenna geometries are demonstrated in Figure 2.25. It has following properties:

- **Curve Length:** The length of the Minkowski curve increases at each iteration. On each iteration, the length of the segments is divided by four and the number of segments is multiplied by eight, hence the total curve length is multiplied by 2 with

each iteration. The length of the curve tends to infinity as the iteration number increases.

- **Fractal Dimension:** The fractal dimension is computed using the Hausdorff-Besicovitch equation:

$$D = \log(N)/log(r) \quad (24)$$

Replacing r by four (as each segment is divided by four on each iteration) and N by eight (as the drawing process yields 8 segments) in the Hausdorff-Besicovitch equation gives:

$$D = \log(8) / \log(4) = 1.5$$

- **Self-Similarity**

Looking at two successive iterations of the drawing process provides graphical evidence that this property is also shared by this curve.

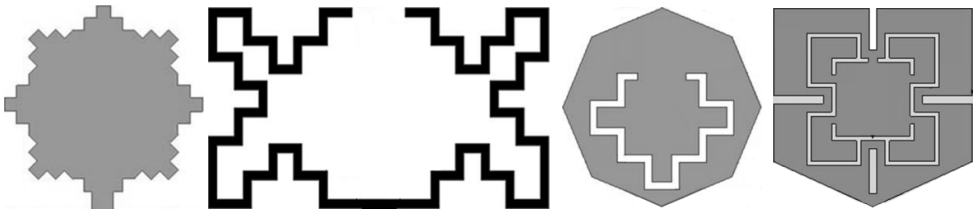

(a) (b) (c) (d)

Figure 2.25 Minkowski antenna geometries

2.6.3.3 Sierpinski Carpet Geometry

Sierpinski Carpet fractal antenna is realized by loading a microstrip radiator with successive iterative slots having same shape as that of initial patch. The initial patch is termed as zeroth iteration. For the first iterative structure, a slot having dimensions equal to initial patch dimensions multiplied by iterative ratio (i.e. 1/2, 1/3, 1/4) is etched at the centre of the zeroth iteration. Thereafter, successive iterative slot dimensions are achieved by scaling down the previous iterative structure dimensions by the same

iterative ratio. The commonly used geometries of initial patch are square, circle, hexagonal etc. [319, 332, 334, 349, 351, 359, 363, 369, 376, 380, 382, 388, 392, 404]. Some of the Sierpinski carpet structures are shown below in Figure 2.26.

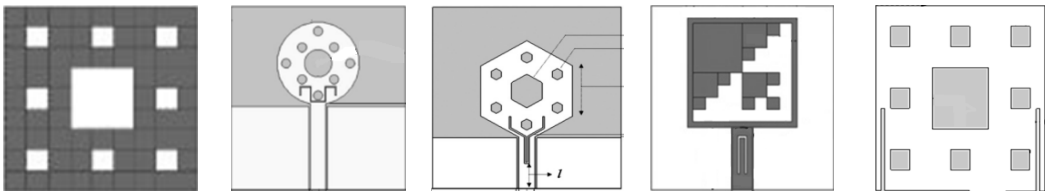

(a) (b) (c) (d) (e)

Figure 2.26 Sierpinski carpet antenna geometries

2.6.3.4 Sierpinski Gasket Geometry

This is the most widely studied fractal geometry for antenna applications. This geometry has been investigated extensively for monopole and dipole antenna configurations. The evolution of this geometry upto second iteration is depicted in Figure 2.27. It is designed by loading a triangular patch with scaled down inverted congruent triangular slot at its centre for first iteration and then loading the resulting triangular portions with further scaled down congruent slots for successive iterations. This process will produce 3^k smaller triangle, and the area is $(3/4)^k$, where k is the number of iterations. The side length of the triangle of each level is half of the side length of the top grade triangle. Some of the Sierpinski gasket antenna structures are presented in Figure 2.28. The iterated function system is as follows [307, 311, 379, 383, 384, 462, 464].

$$\omega(x,y) = \omega_1(x,y) \cup \omega_2(x,y) \cup \omega_3(x,y) \tag{25}$$

Where,

$$\omega_1(x,y) = \left[\frac{1}{2}x, \frac{1}{2}y\right]$$

$$\omega_2(x,y) = \left[\frac{1}{2}x + \frac{1}{4}, \frac{1}{2}y + \frac{\sqrt{3}}{4}\right]$$

$$\omega_3(x,y) = \left[\frac{1}{2}x - \frac{1}{4}, \frac{1}{2}y + \frac{\sqrt{3}}{4}\right]$$

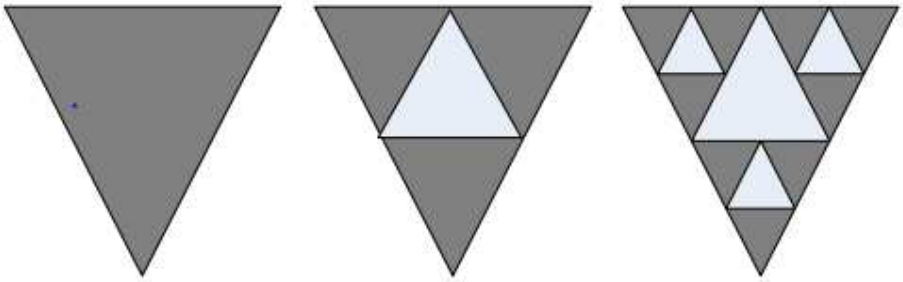

Figure 2.27 Sierpinski gasket for zeroth, first, second iterations

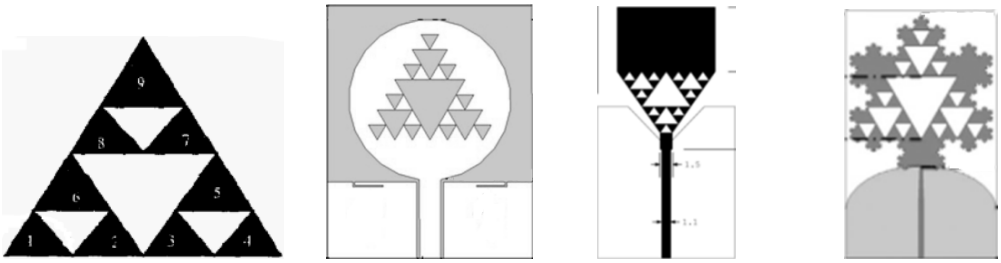

(a) (b) (c) (d)

Figure 2.28 Antenna structures based on Sierpinski gasket geometry

2.6.3.5 Nested type triangular fractal Geometry

Nested type triangular fractal antenna consists of different isosceles triangles with different open angular size and different height and common vertex as shown in Figure 2.29. The shaded area is the antenna entity and the vacuum area is empty area. The number of nested triangles is set *n*, the corresponding height of the triangle is h_1, h_2,...,h_n. Since the nested type triangular fractal antenna contains triangular elements of different sizes, multi-band reflection coefficients of the results appear. The factors which affected the passband center frequency and bandwidth are the height of the nesting triangle, the angle value of the same vertices and the number of nested triangles [462].

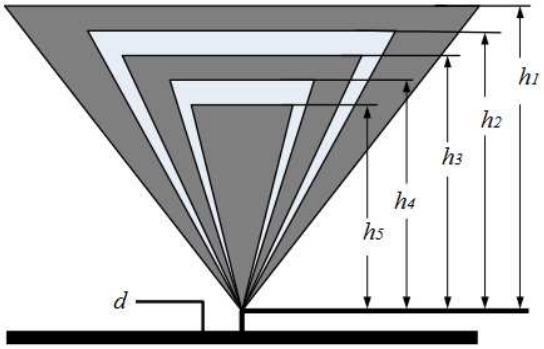

Figure 2.29 Nested triangle fractal antenna structure

2.6.3.6 Hilbert Curves Geometry

It is a space filling curve. It fills the occupied area with increase in iteration number. Three iterations of the Hilbert curve are shown in Figure 2.30. It can be noticed that each successive stage comprises four copies of the previous, connected with additional line segments. This geometry also has the properties of self-Avoidance (as the line segments do not intersect each other), Simplicity (since the curve can be drawn with a single stroke of a pen) and self- Similarity. Because of these properties, these curves are often called as FASS curves [465]. The sum *S* of all the line segments is given by (26).

$$S = (2^{2n} - 1)d = (2^{2n} + 1)L \tag{26}$$

$$d = \frac{L}{2^{n-1}} \tag{27}$$

Here *L* is the side dimension of the Hilbert-curve, *d* is the length of each line segment, and *n* indicates the order of iteration [308, 355, 368, 377, 466].

The approximate equation to calculate the resonant frequency of the Hilbert-curve antenna (HCA) is as follows [368, 466]:

$$\frac{m\eta}{\pi\omega}\left(log\frac{2d}{b}\right)tan(\beta d) + \frac{\mu_o}{\pi}S\left(log\frac{8S}{b} - 1\right) = \frac{\mu_o}{\pi}\frac{k\lambda}{4}\left(log\frac{8}{b}\frac{k\lambda}{4} - 1\right) \tag{28}$$

where λ=2L, m=$4^{(n-1)}$, and b is the diameter of wire, k is an odd integer and η is the intrinsic impedance of free space. The relation equation of between the length of line segment d and resonant frequency f_0 in Eq. (29) can be rewritten as:

$$f_o = \frac{m\eta\left(log\frac{2d}{b}\right)tan(\beta d)}{2\pi\mu_o\left\{\frac{k\lambda}{4}\left(log\frac{8}{b}\frac{k\lambda}{4}-1\right)-S\left(log\frac{8S}{b}-1\right)\right\}} \quad (29)$$

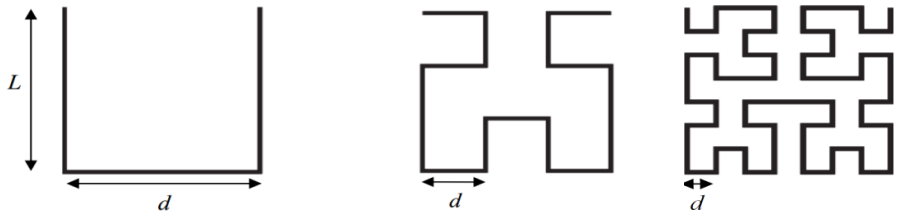

n=0 n=1 n=2

Figure 2.30 Hilbert-curves with increasing iteration order number *n*: (a) First order, (b) second order, and (c) third order

2.6.3.7 Circular Fractal Geometries

The most commonly used geometry for wideband antenna structures is circular geometry due to the excitation of multiple modes and smooth transitions between them along the circular periphery. The zeroth iterative structure or conventional circular patch antenna for a specific resonant frequency is designed by using the following equations:

$$f_r = \frac{1.841v_o}{2\pi r_{eff}\sqrt{\varepsilon_{eff}}} \quad (30)$$

$$r_{eff} = r_o\left[1+\frac{2h}{\pi r_o\varepsilon_r}\left\{ln\left(\frac{r_o}{2h}\right)+(1.41\varepsilon_r+1.77)+\frac{h}{r_o}(0.268\varepsilon_r+1.65)\right\}\right]^{\frac{1}{2}} \quad (31)$$

where, v_o is the velocity of light; r_{eff} is effective radius of circular patch; h is thickness of substrate, ϵ_r is dielectric constant of substrate and r_0 is actual radius of circular patch [315, 317, 330, 336, 339, 340-342, 347, 350, 352, 353, 355, 356, 358, 361, 364, 370, 373, 374, 378, 390, 393-395, 407]. Since the surface current is concentrated at the circumference of the circular patch, so the central portion of the circular patch is loaded

with a slot to achieve the first iteration. In this central slot, another metallic section having geometrical shape like star shape, triangle, square, pentagon etc. is added. Thereafter, this procedure is continued with scaled down version of derived structure in successive iterations. Some circular fractal geometries are shown below in Figure 2.31.

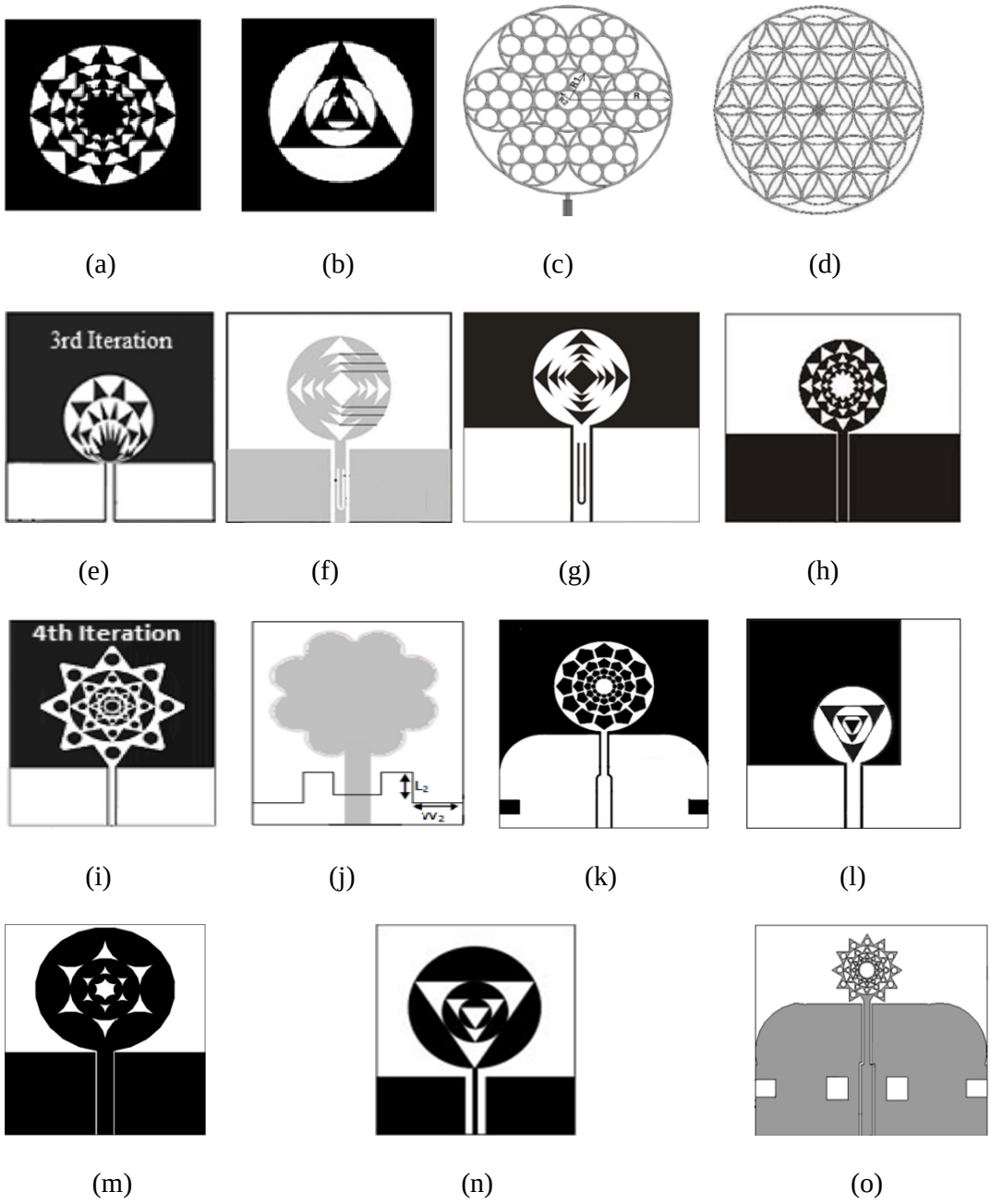

Figure 2.31 Circular fractal antenna geometries

2.6.3.8 Descartes circle theorem

According to complex Descartes theorem, any Descartes configuration of four mutually tangent circles, with curvatures bj and centers $z_j = x_j + iy_j$ satisfies (32)

$$\sum_{j=1}^{4}(b_j z_j)^2 = \frac{1}{2}\left(\sum_{j=1}^{4}(b_j z_j)\right)^2 \tag{32}$$

The complex Descartes theorem also implies a relation connecting the centers of two circles, each of which is tangent to each of three given mutually tangent circles, namely [467]:

$$b_4 z_4 + b_4' z_4' = 2(b_1 z_1 + b_2 z_2 + b_3 z_3) \tag{33}$$

Some of the fractal antenna geometries based on Descarte circle theorem reported in literature [320, 323, 326, 346, 391] are shown below in Figure 2.32.

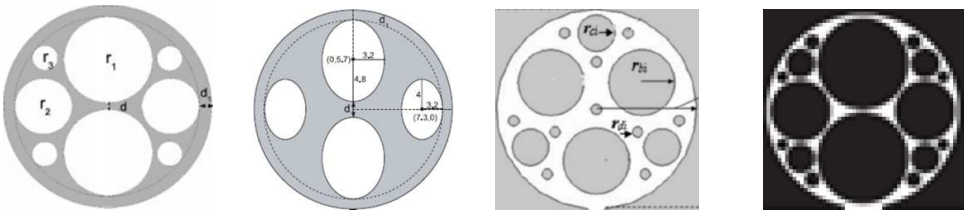

(a) (b) (c) (d)

Figure 2.32 Descartes circle theorem based antenna geometries

2.6.3.9 Giusepe Peano Fractal Geometry

In 1890, Giuseppe Peano introduced a fractal function for space filling property of a structure known as Giuseppe Peano fractal geometry. This concept of Giuseppe Peano fractal structure has been introduced in antenna engineering for miniaturization purpose. The recursive procedure of the Giusepe Peano fractal is shown in Figure 2.33, which is applied to the edges of the square patch up to the second iteration as depicted in Figure 2.33. The Giusepe Peano based antenna geometries [363, 376] are shown in Figure 2.34.

Figure 2.33 Initiator and generator of the Giusepe Peano fractal Geometry

(a) (b)

Figure 2.34 Giusepe Peano based antenna structures

2.6.3.10 Koch Curve Fractal Geometry

A Koch curve is a fractal curve that can be constructed by taking a straight line segment and replacing it with a pattern of multiple line segments. Then the line segments in that pattern are replaced by the same pattern [468]. In the basic Koch curve, a straight line segment is divided into three equal segments and the middle segment is replaced by two line segments of the same length as the segment being replaced with the indentation angle $\theta=60^o$ or 90^o. This is the first iterative structure or generator of Koch curve. Now this procedure of division and replacement is continued to achieve further iterative structures. The stepwise designing of Koch curve is presented in Figure 2.35. A closed geometry constructed from Koch curves is known as Koch Island. For n^{th} iteration of basic triangular Koch island, let N_n be the number of sides, L_n be the length of a single side, l_n be the length of the perimeter, A_n be the area covered after n^{th} iteration. By considering an equilateral triangle of side length, a, and area, A, as the initiator, following equations (34)-(37) are reported in the literature for calculation of Koch curve dimensions. Some antenna structures [306, 309, 314, 321, 331, 338, 343-345, 351, 366, 372, 381, 384, 398] are illustrated below in Figure 2.36.

$$N_n = 3 \times 4^n \tag{34}$$

$$L_n = \left(\frac{1}{3}\right)^n \times a \tag{35}$$

$$l_n = N_n \times L_n = 3 \times \left(\frac{4}{3}\right)^n \times a \tag{36}$$

$$A_n = A_{n-1} + \frac{1}{4} N_n \times {L_n}^2 \times A = A_{n-1} + \frac{1}{3} \times \left(\frac{4}{9}\right)^{n-1} \times A \tag{37}$$

Figure 2.35 Generation of Koch curve upto second iteration

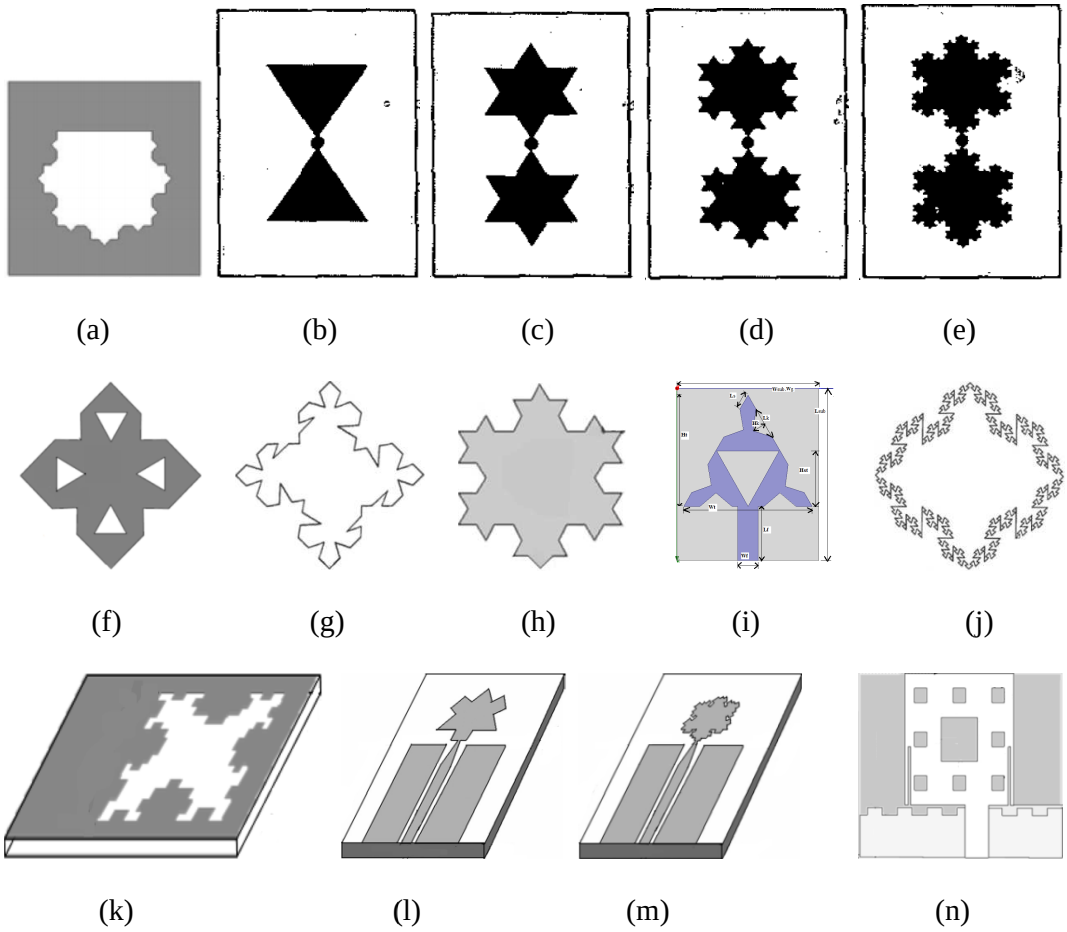

Figure 2.36 Koch curve based antenna structures

2.6.3.11 Pythagorean Tree Fractal Geometry

Pythagoras tree is a 2-D fractal constructed from squares. Its basic structure i.e. Unmodified Pythagoras tree fractal (UPTF) is invented by Dutch mathematician A. E. Bosman in 1942. Each triple of touching squares encloses a right triangle based on configuration traditionally used to depict the Pythagorean Theorem. If the largest square has a size of L×L, the entire Pythagoras tree fits snugly inside a box of size 6L×4L. The construction of the Pythagoras tree begins with a square. Two other squares are constructed upon this square, each scaled down by a linear factor of $(1/2)\sqrt{2}$ such that the corners of the squares coincide pairwise. The same procedure is then applied recursively to the two smaller squares, this process is repeated upto infinity as shown in Figure 2.37. Iteration *n* adds 2^n squares of size $((1/2)\sqrt{2})^n$ in the construction, for a total area of 1. Thus, the area of the tree fractal might seem to grow without boundary $(n \to \infty)$. After fifth iteration, some of the squares get overlapped, and the tree fractal acquires a finite area because it snuggles into a 6×4 box. This overlapping of squares is delayed by eliminating first iteration's large side square and replacing the right angled isosceles triangle with an isosceles triangle having steep angles $\alpha=10^o$, which further miniaturized the antenna dimensions [365]. Figure 2.38 shows an illustration of the first five iterations in the construction process of fractal antenna based on Pythagorean fractal geometry.

Order 0 Order 1 Order 2 Order 3

Figure 2.37 Illustration of the first four iterations for Pythagorean tree fractal

(a) n=0 (b) n=1 (c) n=2

(d) n=3 (e) n=4

Figure 2.38 Fabricated first five iterations for Pythagorean tree fractal monopole antenna

2.6.3.12 Tree Shaped Fractal Geometries

2.6.3.12.1 Basic tree shaped fractal

Basic structure for tree shaped fractal geometry is simple rectangular patch antenna. Then rectangular initiator is scaled down and repeated up to second iteration. The iterative structures are arranged in a manner that the overall structure looks like a tree. All three iterations [322, 325] were connected to achieve the final tree shaped fractal antenna as show in Figure 2.39. The rectangular patch can be replaced by a trapezoidal patch also to design a tree shaped fractal antenna [322, 325].

(a) Rectangular (b) Trapezoidal

Figure 2.39 Tree shaped fractal geometries

2.6.3.12.2 Fractal Binary tree Geometry

A binary fractal tree is defined recursively by symmetrical binary branching. Here, the approach taken for the generation of trees is somewhat different from conventional fractal shapes. One starts with a "stem" and allows one of its ends to branch off in two directions. In the next iteration, each of these branches are allowed to branch out again, and this process is continued infinitely as shown in Figure 2.40. Figure 2.41 shows 3rd iterative fractal binary tree with different branching angles [333, 357, 375, 387, 399, 400, 411]. The antenna structures based on binary tree geometry reported in literature are shown in Figure 2.42.

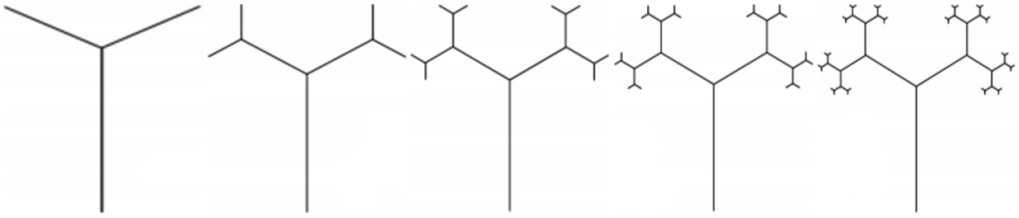

Figure 2.40 Various iterations of fractal Binary tree.

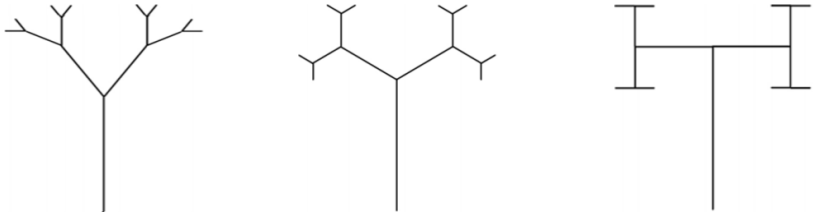

60° 120° 180°

Figure 2.41 3rd iterated fractal Binary tree with different branching angles

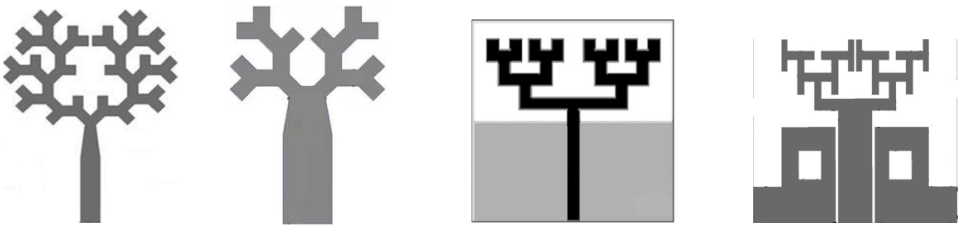

(a) (b) (c) (d)

Figure 2.42 Different binary tree antenna geometries

2.6.3.13 Penta-Gasket-Khoch (PGK) fractal

The zeroth iteration of this geometry is a regular pentagon. This pentagon is loaded with five congruent isosceles triangular slots, which results into first iterative structure having five triangular slots and one pentagonal slot at the centre of initial pentagon. This slot loading procedure is carried out repetitively on every pentagonal structure to achieve further iterative structures. The antenna geometry is presented in Figure 2.43. Another fractal geometry based on Penta Gasket Khoch concept is its complement i.e. Complementary Penta Gasket Khoch (CPGK) fractal geometry. In this geometry, the slots have the shape of pentagons [318, 321, 367]. The antenna configuration is demonstrated in Figure 2.44.

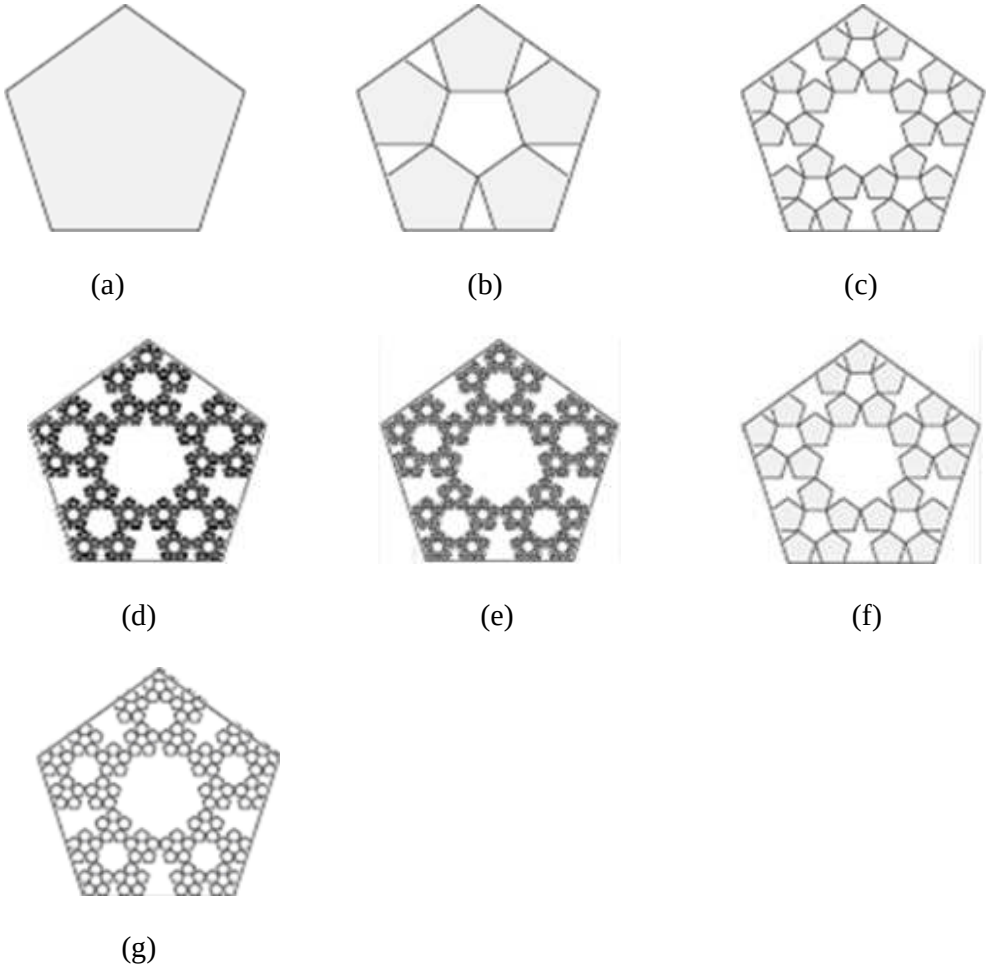

Figure 2.43 Penta-Gasket-Khoch (PGK) antenna up to fifth iteration.

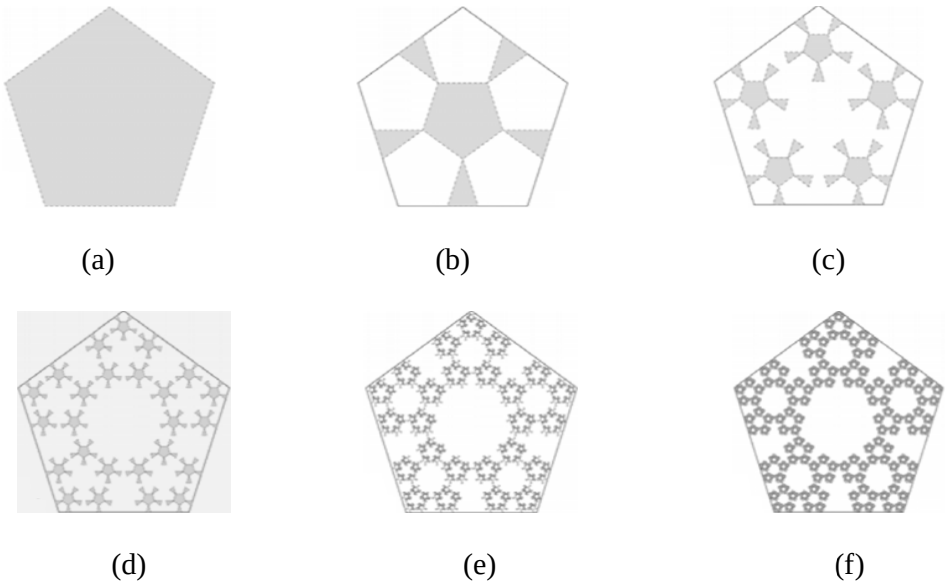

Figure 2.44 Complementary Penta Gasket Khoch (CPGK) antenna up to fifth iteration.

2.6.3.14 Kernel Array of Microstrip Patches (ReKAMP)

A Repeated Kernel Array of microstrip Antenna (ReKAMP) [311] is generated by following a systematic procedure as follows:

A certain microscopic kernel is repeated according to a certain rule such that it draws a shape similar to itself but on a macroscopic separation skeleton. The geometry of the resulting shape is best described as being the result of repeating the operation $X^i = Rule(X^{i-1})$ as many times as the number of stages required. At the beginning of the procedure X is the initiating kernel and at the end procedure X is the resulting ReKAMP. There are two pre-defined classes of ReKAMPs: Coupled kernel ReKAMPs and Connected kernel ReKAMPs.

1. For coupled kernel ReKAMPs, the rule consists of simple repetition of the kernel on the vertices of a similar shape (the repetition skeleton) without any direct connection between the repeated kernels.
2. For connected kernel ReKAMPs, the rule involved in the generation process is "repeat and connect" rule i.e. the kernels are repeated on the vertices of a similar

shape such that direct connections are established between the repeated kernels on the perimeter of that similar shape during the repetition phase of the rule.

The ReKAMP antenna geometries are demonstrated in Figure 2.45.

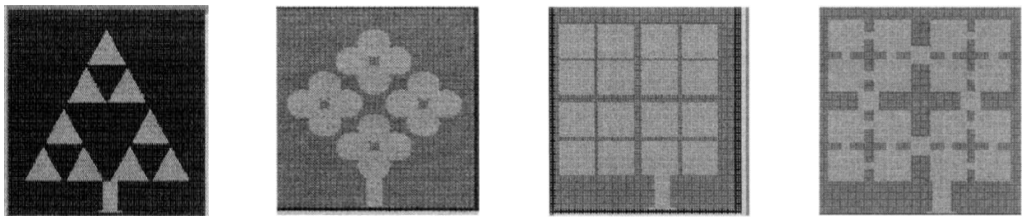

(a) (b) (c) (d)

Figure 2.45 Different ReKAMP geometries (a) Triangular, (b) circular, (c) square coupled, (d) square connected.

2.6.3.15 Square fractal geometries

Similar to circular fractal geometry, square fractal geometry is also used to design antenna structures. The square shaped radiating patch is loaded with a geometrical slot for first iteration. This iterative structure is scaled down and inserted in the slot of previous iteration structure [313, 329, 335, 362]. The square fractal antenna structures are depicted in Figure 2.46.

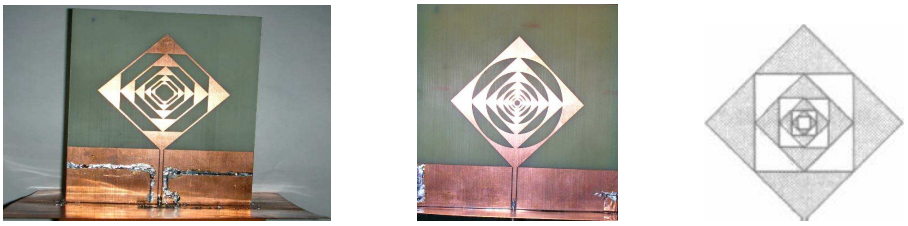

(a) (b) (c)

Figure 2.46 Square fractal antenna geometries

2.6.3.16 Cantor Set fractal geometry

The geometry of the proposed antenna is based on the geometry of Cantor set. A Cantor set is a self-similar object which is formed by an iterative process starting with initiator of length and width. First, the initiator is partitioned in to three non overlapping

segments with the middle segments removed. This process is continued by repetitive application of the generator to each remaining layer. This is described using Iteration function system represented by self affine transformation. The generation of Cantor set fractal geometry [360, 371, 385, 469] is shown in Figure 2.47. The n^{th} set is represented as

$$C_n = \frac{C_{n-1}}{3} \cup \left(\frac{2}{3} + \frac{C_{n-1}}{3}\right) \tag{38}$$

$$C_0 = [0, 1] \tag{39}$$

The Cantor ternary set contains all points in the interval [0, 1] that are not deleted at any step in this infinite process. An explicit closed formula for the Cantor set is

$$C = \bigcap_{m=1}^{\infty} \bigcap_{k=0}^{3^{m-1}-1} \left(\left[0, \frac{3k+1}{3^m}\right] \bigcup \left[\frac{3k+2}{3^m}, 1\right]\right) \tag{40}$$

$$C = [0,1] \backslash \bigcup_{m=1}^{\infty} \bigcup_{k=0}^{3^{m-1}-1} \left(\frac{3k+1}{3^m}, \frac{3k+2}{3^m}\right) \tag{41}$$

Since the Cantor set is defined as the set of points not excluded, the proportion (i.e., measure) of the unit interval remaining can be found by total length removed. This total is the geometric progression

$$\sum_{n=0}^{\infty} \frac{2^n}{3^{n+1}} = \frac{1}{3}\left(\frac{1}{1-\frac{2}{3}}\right) = 1 \tag{42}$$

So that the proportion left is 1 - 1 = 0.

Properties of Cantor Set fractal geometry:

1. **Uncountable:** In a Cantor set, the number of points left after the geometry design is equal to the number of points from which further iterations can be designed.
2. **Cardinality:** Its cardinality is no less than [0,1]

3. **Self-similarity:** It is self-similar, because it is equal to two copies of itself, if each copy is shrunk by a factor of 3 and translated.

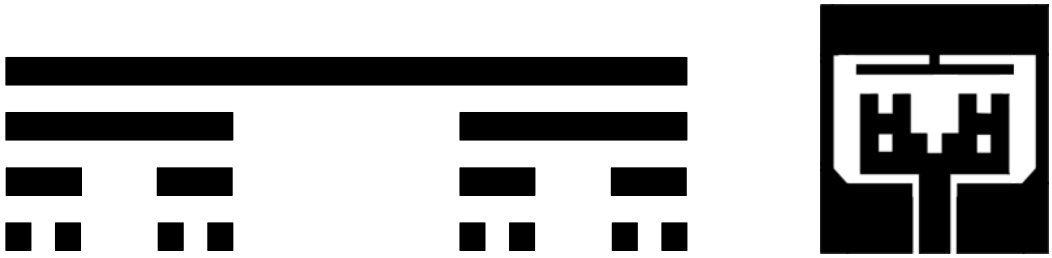

(a) (b)

Figure 2.47 (a) Basic cantor set generation (b) Cantor geometry.

2.6.3.17 Other geometries

In addition to above mentioned fractal geometries, some more fractal antenna geometries are designed by using the properties of self-similarity and space filling properties. The fractal antenna geometries [310, 312, 316, 324, 327, 328, 337, 348, 354, 389, 396, 397, 405, 406, 408, 409] reported in literature are shown below in Figure 2.48 and Figure 2.49.

(a) (b) (c)

Figure 2.48 (a) Rectangular Fractal monopole (b) Fractal triangular monopole with same vertex, (c) Fractal triangular monopole with same slope.

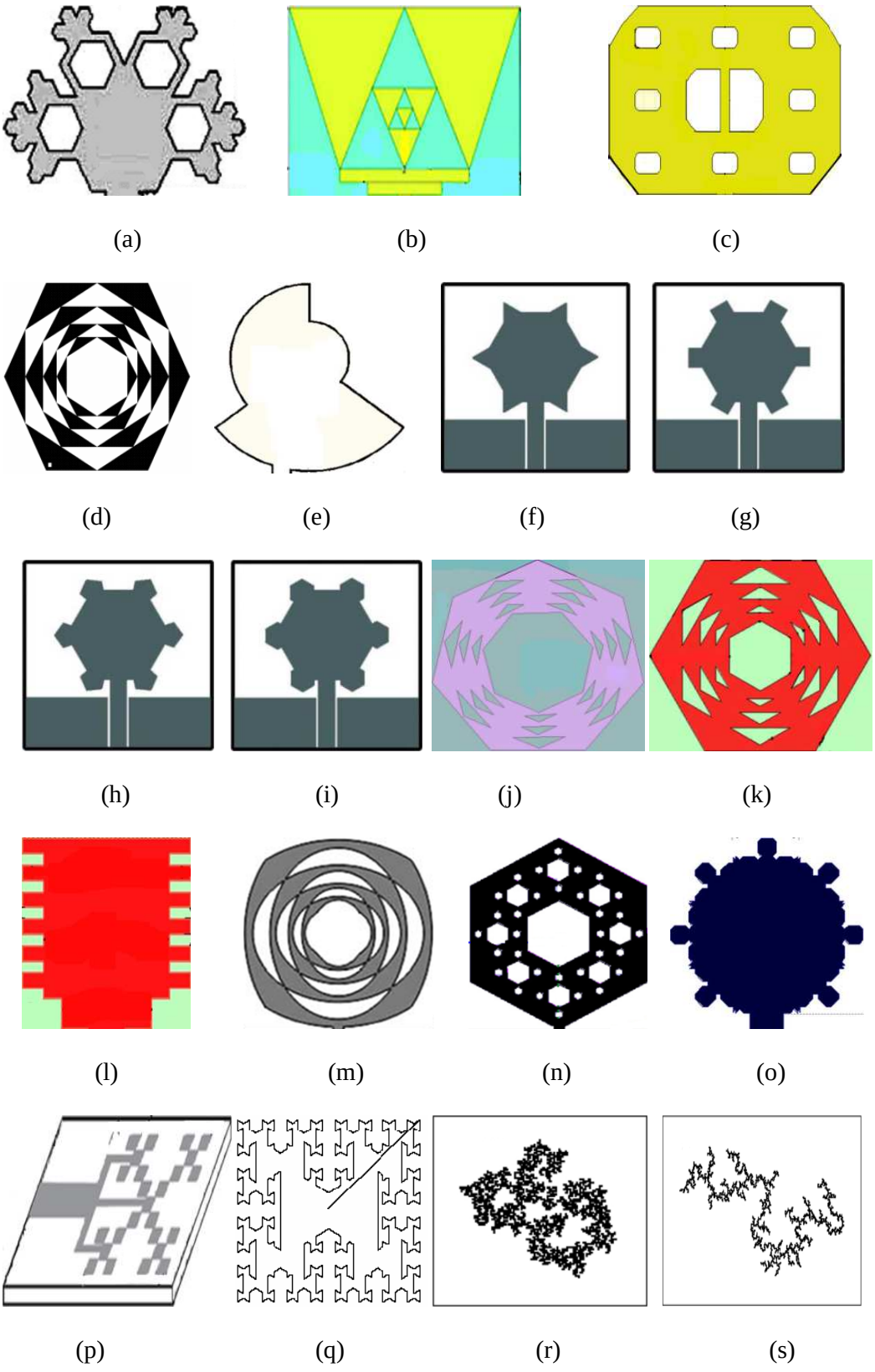

Figure 2.49 Different fractal antenna geometries

2.6.4 General Applications of Fractal

2.6.4.1 Astronomy

Fractals will revolutionize the way that the universe is seen. Cosmologists usually assume that matter is spread uniformly across space. But observation shows that this is not true. Astronomers agree with that assumption on "small" scales, but most of them think that the universe is smooth at very large scales. However, a dissident group of scientists' claims that the structure of the universe is fractal at all scales.

2.6.4.2 Computer Science

Use of fractals in computer science is the fractal image compression. This kind of compression uses the fact that the real world is well described by fractal geometry. By this way, images are compressed much more than by usual ways (e.g. JPEG or GIF file formats). Another advantage of fractal compression is that when the picture is enlarged, there is no pixelization. The picture seems very often better when its size is increased.

2.6.4.3 Fluid Mechanics

The study of turbulence in flows is very adapted to fractals. Turbulent flows are chaotic and very difficult to model correctly. A fractal representation of them helps engineers and physicists to better understand complex flows. Flames can also be simulated. Porous media have a very complex geometry and are well represented by fractal. This is actually used in petroleum science.

2.6.4.4 Wireless Communication

The space saving abilities of fractals are to efficiently fill a limited amount of space which create distinct advantage of using integrated fractal over Euclidean geometry. Examples of these types of application include personal hand-held wireless

devices such as cell phones and other wireless mobile devices such as laptops on wireless LANs and networkable PDAs. This area has many possibilities arranging from dual-mode phones to devices integrating communication and location services such as GPS, the global positioning satellites. Fractal also decrease the area of a resonant antenna, which could lower the radar cross-section (RCS). This benefit can be exploited in military applications where the RCS of the antenna is a very crucial parameter.

2.6.5 Advantages of Fractal antenna

Fractal also provides many versatile capabilities. They can be extremely small for applications requiring an embedded antenna, or contained in transparent materials to achieve near-invisible larger-scale form factors. The following

Table 2.2 highlights the features and benefits of Fractal Antenna Systems technology.

Table 2.2 Feature, advantages and benefits of fractal

Feature	**Advantage**	**Benefit**
Multiband /Wideband	Instantaneous access of spectrum	Use single antenna instead of many
Low Mutual Coupling	Close packing	Small arrays with excellent steer ability
New design space	Powerful solutions possible	Design to requirements, not pick from catalog
Fractal ground plane/counterpoise	Smaller, multiband	Greater versatility, new packaging options
Frequency independency	Consistent performance over wide frequency range	Fractal solutions open up previously unknown options
Loading of Fractal	Added capacitance and inductance without components	Enables small, efficient, reliable communication
Very Compact	Using of versatility and More design	Reduces cost and enhances desirability
Proven Products	Designed for harshest conditions	In use by military and commercial customers

2.7 Dipole Antenna

A dipole antenna is a straight electrical conductor measuring λ/2 between end to end and its centre is connected to a radio-frequency (RF) feed line. The radio frequency current flows between the two terminals of dipole antenna. Due to this current and associated voltage, electromagnetic or radio signal is radiated. The basic dipole antenna is shown in Figure 2.50.

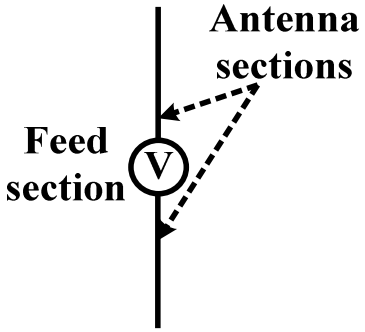

Figure 2.50 Basic dipole antenna

Since, two arms of the dipole antenna are identical and symmetrical to the feed, the phase distribution on each conductive arm of the dipole is constant, and the open end is seen as an open circuit from the feeding terminal. In an ideal situation, the current reaches zero at the open end of the arms. Radiation from each segment of the antenna arms has different phase delays, due to the physical length of the arms [470-471]. The antenna pattern factor *F* (θ) is mathematically calculated by equation

$$F\ (\theta) = \frac{cos\left(\frac{1}{2}kl\,cos(\theta)\right) - cos\left(\frac{1}{2}kl\right)}{sin\,\theta} \tag{43}$$

$$k = \frac{2\pi}{\lambda} \tag{44}$$

where *k* is the wave number and *l* is the length of the wire. Thus, it is clear that the physical length of a dipole antenna and wavelength have critical effects on the antenna

pattern factor. The length of the radiating element plays a significant role in determining many properties of the dipole antenna like impedance, centre operating frequency, etc.

A dipole antenna or half wave dipole forms a resonant circuit, which resonates where the electrical length is equal to half of wavelength. These resonant circuit characteristics lead to narrow bandwidth. In present scenario, there is requirement of ultra wideband antenna structures. Several techniques have been reported in the literature to enhance the dipole antenna bandwidth.

UWB planar dipole antenna structures are low cost, low profile and suitable for integration with feed network. They have omnidirectional radiation patterns, substantially smaller dimensions and turn out to be more suitable for any communication device e. g. radar, positioning devices etc. They have high input impedance which facilitates the impedance matching easily. The disadvantages of dipole antenna are less gain, non-directionality and large size. UWB planar dipole antenna is a suitable candidate for ground penetrating radar and short range communication applications.

2.7.1 UWB Dipole Antenna Geometries

The reported dipole antenna geometries can be subdivided into two categories i.e. uniplanar and double printed. Uniplanar geometries consist both dipole arms on the same side of the substrate i.e. dipole arms are coplanar. These structures are easy to fabricate and have low cost but they require additional impedance matching circuitry. Double printed geometries comprise one dipole arm on each side of the substrate. These structure resolve the problem of impedance matching faced in uniplanar geometries. Some of these geometries are being discussed below.

2.7.1.1 Uniplanar dipole antenna with single feed location

If both the dipole arms of a dipole antenna are fed from a common location then there will be no difference between the amplitude and phase of excitation signal for both arms. Several dipole antenna structures having their both dipole arms on the same plane and having common feed location [414, 426, 429, 435, 438, 451, 452] are reported in the literature. Single feed location dipole antenna geometries are presented in Figure 2.51.

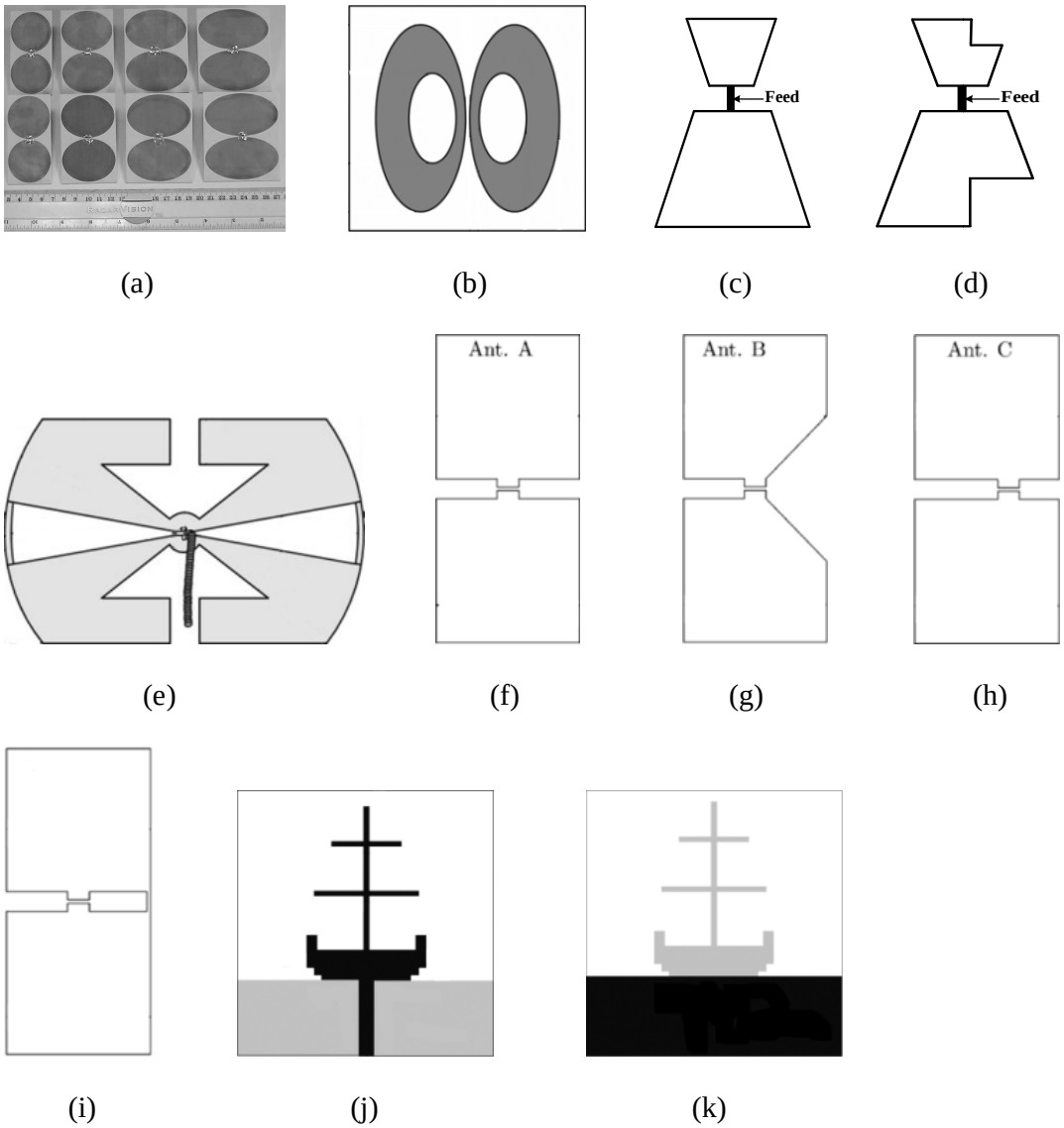

Figure 2.51 Geometries of uniplanar dipole antenna with single feed location

2.7.1.2 Uniplanar dipole antenna with shorted dipole arms

To miniaturize the dipole antenna geometry with improvement in impedance bandwidth and radiation characteristics, dipole arms are being shorted by using shorting strips. The use of these shorting strips increases the electrical length of radiating elements without increasing the overall antenna size. Some of the antenna structures have single feed location whereas separate feedlines i.e. coplanar strip line [429, 435, 474]. Antenna structures are depicted in Figure 2.52.

2.7.1.3 Uniplanar dipole antenna with balun

To feed an elliptical dipole antenna, one needs to supply power from a source generator via a coaxial cable or microstrip line. However, the coaxial cable and microstrip line are unbalanced transmission lines. Due to these unbalanced transmission lines, the antenna pattern are accessible by undesired cable currents. As a solution this problem, a balun structure is used to provide a broadband unbalance-to-balance transition. Some dipole antenna configurations with balun [428, 430, 441, 472, 475] reported in literature are demonstrated in Figure 2.53.

2.7.1.4 Uniplanar dipole antenna with coplanar strip line

Dipole antenna with coplanar strip line [444, 475] could be used as differential antenna and could be directly connected to a differential circuit. The elliptical dipoles with feeding lines on the same plane as the radiating elliptical elements find an easier way of connecting the antenna to the UWB circuit and to etch the antenna on the same PCB as the circuit. Antenna geometries are presented in Figure 2.54.

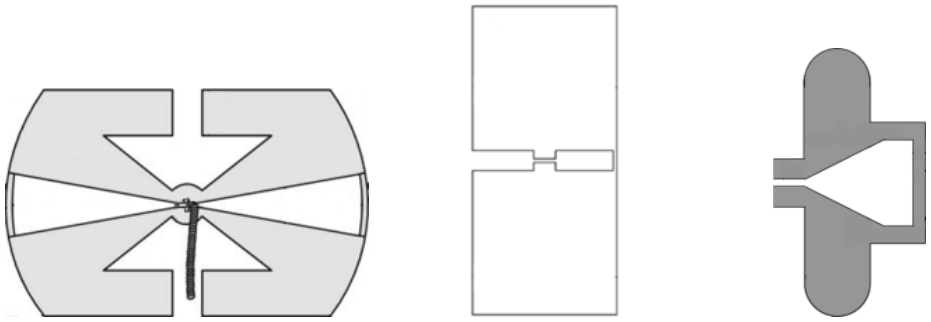

(a) (b) (c)

Figure 2.52 Geometries of uniplanar dipole antenna with shorted dipole arms

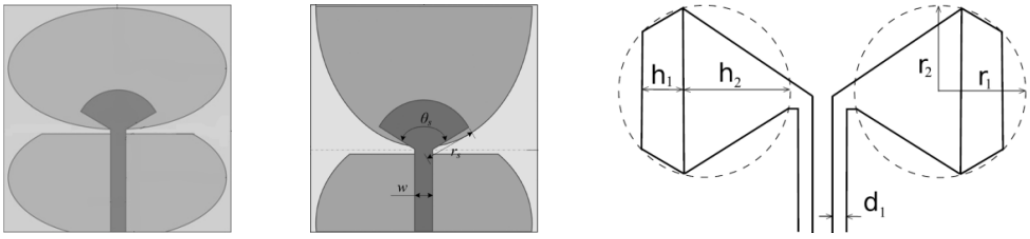

(a) (b) (c)

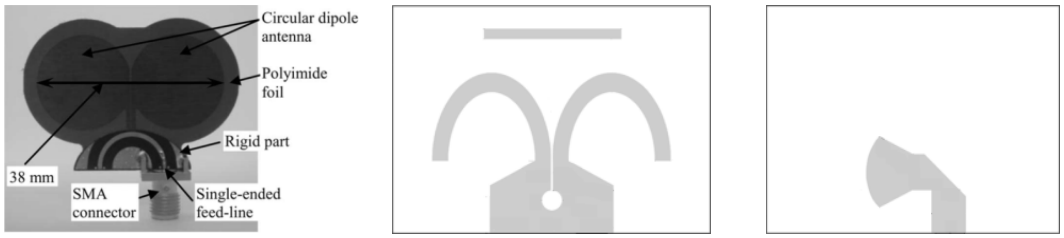

(d) (e) (f)

Figure 2.53 Geometries of uniplanar dipole antenna with balun

(a) (b)

Figure 2.54 Geometries of uniplanar dipole antenna with coplanar strip line

2.7.1.5 Uniplanar dipole antenna with tapered slot feed and parasitic element

Ma and Jeng [428] presented an antenna having wide-band tapered-slot feeding structure, curved radiators and a parasitic element as shown in Figure 2.55. Tapered slot antenna may become unsatisfactory in UWB systems due to their inherently directional patterns. The pair of curved strips was used to radiate energy more evenly over the space. The parasitic element in front of the feeding aperture enhanced the in-band impedance matching by changing the current distribution of the radiators. Antenna geometries is shown in Figure 2.55.

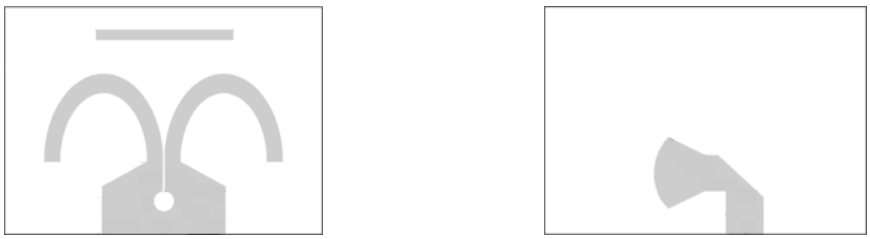

(a) Top layer (b) Bottom layer

Figure 2.55 Geometry of uniplanar dipole antenna with tapered slot feed and parasitic element

2.7.1.6 Double printed dipole antenna geometries

In addition to uniplanar dipole geometries, another dipole geometry which is being designed for UWB applications is double printed antenna geometry. In these geometries, one half of the antenna is printed on the top surface of the substrate layer and connected to the feedline, while the second half is placed on the bottom substrate layer and connected to the ground plane. Doing that avoids using balun and simplifies the antenna geometry. In double printed antenna, one dipole arm is printed on each side of the substrate material. The double printed UWB dipole geometries [416, 431, 433, 442, 443, 448, 450, 454] reported in the literature have utilized techniques of stepped

feedlines, baluns, different shapes of dipole elements, slot or notch loading of the dipole arms, half mode substrate integrated waveguide (HMSIW) balun [473] etc. to achieve wide bandwidth or band notch characteristics. Double printed antenna geometries are illustrated in Figure 2.56.

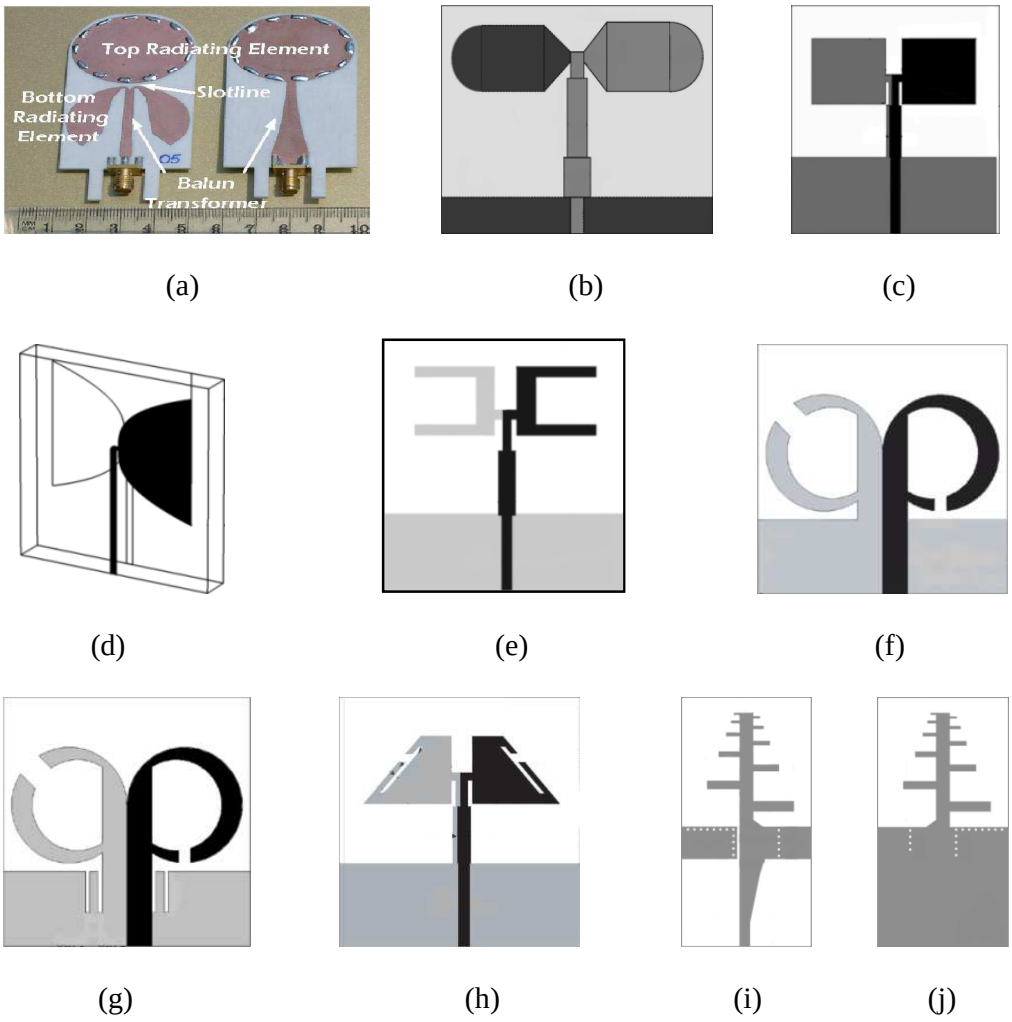

Figure 2.56 Geometries of double-printed dipole antenna structures

After the detailed study of literature survey of various methods, geometries etc. used to design planar antennas for UWB applications already reported in the literature, the design and analysis of fractal antenna structure is taken up in detail in next chapter.